

# Lawrence Berkeley National Laboratory

## Recent Work

### Title

The hydrogen electrode reaction and the electrooxidation of CO and H<sub>2</sub>/CO mixtures on well-characterized Pt and Pt-bimetallic surfaces

### Permalink

<https://escholarship.org/uc/item/26m716qt>

### Author

Markovic, N.M.

### Publication Date

2001-12-01

# The hydrogen electrode reaction and the electrooxidation of CO and H<sub>2</sub>/CO mixtures on well-characterized Pt and Pt-bimetallic surfaces

N. M. Marković

Materials Sciences Division, Lawrence Berkeley National Laboratory  
University of California Berkeley, CA 94720

## Abstract

Interrelationships between the kinetics of fuel cell reactions and the structure/composition of anode catalysts are reviewed. Model systems like Pt single crystals and well characterized Pt(hkl)-Pd and Pt<sub>3</sub>Sn(hkl) bimetallic surfaces are used to establish a link between the macroscopic kinetic rates and thermodynamic properties of the reacting system and the microscopic level of understanding the bonding and reactivity of reaction intermediates and spectator species. The results show that the hydrogen reaction is structure sensitive process, with Pt(110) being an order of magnitude more active than either of the atomically “flatter” (100) and (111) surfaces. The difference in activity with crystal face is attributed to the structure sensitive adsorption of hydrogen (H<sub>upd</sub>) and hydroxyl anions (OH<sub>ad</sub>) and the effect these species have on the formation of active intermediate (H<sub>opd</sub>). The significant differences of the hydrogen reaction in alkaline versus acid electrolytes are suggested to arise due to the presence of OH<sub>ad</sub> even close to the reversible potential of the hydrogen reaction in alkaline electrolyte. The hydrogen reaction on Pt(hkl) modified by pseudomorphic Pd (sub)monolayers shows the “volcano-like” behavior, having the maximum rate on Pt(111) modified by 1 ML of Pd. The physical model based on differences in the adsorption energies of H<sub>upd</sub> and H<sub>opd</sub> on Pd vs. Pt is used to rationalize the catalytic activity of Pd atoms. For the Pt(111)-CO system, a remarkable difference in both activity and stability of the p(2x2)3CO ordered structures is observed between alkaline and acid solutions. The pH-effect is explained as the pH-dependent adsorption of OH<sub>ad</sub>, which starts in the H<sub>upd</sub> potential region at defect sites. The oxidation of H<sub>2</sub> in the presence of CO occurs concurrently with CO oxidation on Pt and Pt bimetallic surfaces. The Pt<sub>3</sub>-Sn(hkl) system is used to demonstrate that both the bifunctional effect and the ligand effect contribute to the influence of Sn on the CO oxidation rate and for H<sub>2</sub> oxidation process in the presence of CO.

*Keywords:* Hydrogen reaction, CO oxidation, H<sub>2</sub>/CO mixtures, Electrocatalysis, Bifunctional effect, Electronic effect, Single crystals, Surface structure, Surface morphology, Bimetallic alloys, Platinum, Palladium, Tin, Ruthenium, Molybdenum.

#### 4.2.1. Introduction

A device for direct conversion of chemical energy into electrical energy, i.e. a full cell, was described by Grove [1] well before either the internal combustion engine or the steam-generator were developed. At the beginning of 20<sup>th</sup> century, however, it was the heat engine rather than the electrochemical engine which was chosen as the main source of motive power, although the latter offered theoretically higher efficiency. A slow development of fuel cells was mainly influenced by the lack of understanding why an electrochemical converter has efficiency which was, in practice, no better than this of an internal combustion engine. Almost six decades later, when scientists realized that the losses in electrochemical energy converters are extrinsic and that can be reduced by improving the knowledge in the field of electrocatalysis, we have witnessed a resurgence of interest in fuel cell technology. Historically, the development of catalysts for fuel cells has been mostly empirical and virtually all of the catalysts used today were developed at the beginning of 1960s. The early 1990s represents a second landmark in the experimental and theoretical development of new electrocatalysts for fuel cell reactions. Model system like single crystal electrodes and well-characterized alloy surfaces were studied to create a link between the microscopic properties of the adsorption sites of reactants and intermediates and macroscopic measurements of kinetic rates of the reacting system. The knowledge is then used to create tailor-made surfaces having the required microscopic structure to produce the desired catalytic properties. The number of publications concerned with the materials-by-design approach to development of new catalysts for fuel cell reactions is far too extensive to cite adequately in a limited survey. A large number of review articles are, however, already available and in this chapter these are cited as guides to the earlier literature. In the present chapter an attempt will be made to upgrade previous reviews, with emphasis on the most recent developments in the electrocatalysis of the hydrogen reaction, the electrooxidation of carbon monoxide, and the electrooxidation of H<sub>2</sub>/CO mixtures on well-characterized Pt and Pt-bimetallic surfaces. As background for discussion, the structure sensitive adsorption of hydrogen, oxygenated species, and anions on platinum single crystal surfaces in aqueous solutions is presented. After summarizing the thermodynamics of reactive intermediates and spectator species, it will be shown that the kinetics of the hydrogen reaction vary with the

surface structure, emphasizing that if special sites are needed for adsorption then special sites are also needed for reaction. The next section reviews the kinetics of the hydrogen reaction at Pt bimetallic surfaces. The Pt(111)-Pd system is used to demonstrate how the energetics of intermediates formed in the hydrogen reaction is affected by interfacial bonding and energetic constraints produced between pseudomorphic Pd films and the Pt(111) substrate. The final sections discuss the kinetics of oxidation of CO and H<sub>2</sub>/CO mixtures on Pt and Pt-Sn bimetallic alloys. An introduction to the relation of structure stability and catalytic activity of the adsorbed CO on Pt(111) to the nature of anions present in the supporting electrolytes is given to demonstrate the relationship between the atomic-scale structure of the model catalysts and adsorption sites of reactants and spectator species. This approach has been extremely successful in the development of more active catalysts for CO oxidation by tailoring the properties of Pt-binary alloy surfaces for the adsorption of CO onto specific states and by alloying Pt with more oxyphilic metals. Although the catalytic activity of Pt can be greatly enhanced by the addition of Ru, Sn, Mo and Re, only the tailor-made Pt<sub>3</sub>Sn(111) surface will be discussed in this chapter.

#### **4.2.2 HER/HOR on Pt(hkl) and Pt(hkl) bimetallic surfaces**

The hydrogen evolution reaction (HER) and the hydrogen oxidation reaction (HOR) are among the most widely studied electrochemical processes. All the basic laws of electrode kinetics as well as the modern concepts in electrocatalysis were developed and verified by examining the hydrogen reaction [2],



The intrinsic kinetic rate of this reaction, termed the exchange current density,  $i_0$ , is defined as the rate at which the reaction proceeds at the equilibrium (zero net current) potential. The exchange current density for the hydrogen reaction varies by 5-6 orders of magnitude depending on the electrode material. Attempts to correlate the exchange current density of the hydrogen reaction with the properties of the electrode substrate date back several decades. A breakthrough with regards to the relationship between  $\log i_0$  and physical properties of the electrode substrates was achieved in 1957 when Conway and Bockris demonstrated a linear functionality between  $\log i_0$  and the metal's

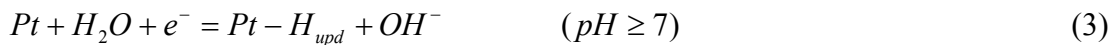
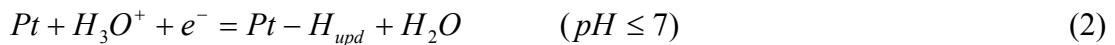
work function,  $\Phi$ , and attributed this to the relation between  $\Phi$  and the metal-hydrogen interaction energy [3]. In the meantime, Parsons [4] and Gerischer [5] independently established from the classical transition state theory the correlation between  $\log i_0$  and the Gibbs energy of adsorbed hydrogen ( $\Delta G_{Had}^0$ ). The general form of this relation possesses a “volcano” shape with the maximum of  $\log i_0$  values arising at  $\Delta G_{Had}^0 = 0$ . The highest exchange current density is exhibited by Pt on which hydrogen is adsorbed to a moderate extent. Two decades later, based on the relationship between  $\log i_0$  and the M-H<sub>ad</sub> bond energy, Trasatti demonstrated that the volcano plot for the HER is valid for both metals and non-metals [6,7]. In all previous measurements for constructing volcano plots,  $\Delta G_{Had}^0$  was inferred from gas phase data in low pressure conditions, and Pt was classified among the group of metals with  $\Delta G_{Had}^0 < 0$ . Protopopoff and Marcus, however, suggested that Pt should be correlated with the gas-phase data for dissociative adsorption of H<sub>2</sub> in high pressure conditions (since the HER begins at an equivalent pressure of  $\approx 1$  atm), and therefore Pt should be classified among the group of metals with  $\Delta G_{Had}^0 > 0$  [8]. Although the Protopopoff-Marcus approach has made a big impact in rationalizing the position of Pt in the volcano plot, at the beginning of 1990’s many important questions concerning the hydrogen reaction still remained open: (i) Is the hydrogen reaction a structure-sensitive process? (ii) What is the relationship between the reaction intermediate (the so-called overpotentially deposited hydrogen, H<sub>opd</sub>) and the underpotentially deposited hydrogen, H<sub>upd</sub>? (iii) Why is the rate of the HER/HOR significantly lower in alkaline than in acid electrolytes? (iv) How does the adsorption of hydrogen affect the kinetics of the hydrogen reaction?

The present section will attempt to answer some of these questions and hopefully illustrate that it is quite feasible to “tune” the kinetics of the HER/HOR by systematic changing of the arrangement of platinum surface atoms and/or by tailor-making Pt(hkl)-Pd bimetallic surfaces.

#### 4.2.2.1 *H<sub>upd</sub>, OH<sub>ad</sub> and anions adsorption on Pt(hkl) surfaces*

Ever since the pioneering work of Will [9], one of the major themes in surface electrochemistry has been the study of the relationship between electrochemical reactivity and surface structure, a functionality generally termed “structure sensitivity”. In electrochemical experiments well-defined Pt(hkl) single crystal electrodes can be prepared either by conventional sputtering and annealing treatment in UHV [10-13] or by annealing the single crystal in an open hydrogen-air flame [14-17]. Direct evidence that a relatively simple and fast flame-annealing method can be used for preparation of well-ordered Pt(111)-(1 x 1) (with Pt atom surface density  $\rho = 1.53 \times 10^{15}$  atoms/cm<sup>2</sup>), Pt(100)-(1x1) ( $\rho = 1.28 \times 10^{15}$  atoms/cm<sup>2</sup>), and Pt(110)-(1x2) ( $\rho = 0.94 \times 10^{15}$  atoms/cm<sup>2</sup>) surfaces was obtained from in-situ SXS [18,19] and STM [17,20-22] measurements. For brevity, Pt(111)-(1x1), Pt(100)-(1x1) and Pt(110)-(1x2) surfaces will be denoted just as Pt(111), Pt(100), and Pt(110) hereafter. The in-situ SXS technique has been a critical tool to demonstrate that, between the potential region of the hydrogen evolution reaction and the onset of irreversible “oxide” formation, Pt(111), Pt(100) and Pt(110) are stable and do not exhibit potential-induced reconstruction, which is characteristic on the Au(hkl)-electrolyte systems [23-25]. As a result, electrochemical surface processes on Pt(hkl) can be examined on the geometrically simple surfaces having well-known individual adsorption sites. The most simplified system to demonstrate that each Pt single crystal exhibits its own singular surface (electro)chemistry is the adsorption of hydrogen and oxygen containing species on Pt(hkl) in alkaline solution. As shown in Figure 1, the adsorption of both H<sub>upd</sub> and oxygenated species varies with crystal face, confirming that Pt-adsorbate energetics is uniquely determined by the arrangement of surface atoms.

As in UHV [26], the energetics of Pt-H<sub>upd</sub> can be derived from measurements of the equilibrium coverage by H<sub>upd</sub> as a function of temperature, Figure 2. Depending on the pH of solution, H<sub>upd</sub> is generated either from protons or water molecules:



Unfortunately, because of the close coupling between anions and  $H_{\text{upd}}$  adsorption on Pt(100) and Pt(110), the determination of Pt- $H_{\text{upd}}$  energetics on these two surfaces is problematic in both acid and alkaline solutions [27,28]. On the other hand, considering that the co-adsorption of  $H_{\text{upd}}$  and anions on Pt(111) is relatively small, the thermodynamic state functions for  $H_{\text{upd}}$  at Pt(111) can be assessed from the experimentally measured  $\Theta_{H_{\text{upd}}}$  vs. T dependence (Figure 2a) when the electrode potential is referenced to the potential of the reversible hydrogen electrode,  $E_{\text{rhe}}$ , in the same electrolyte at the same temperature [27-29]. This methodology was adopted from original works by Breiter [30,31] and Conway [32-34] for the measurements of the thermodynamic state functions for  $H_{\text{upd}}$  on polycrystalline Pt electrode. For the Pt(111)- $H_{\text{upd}}$  system, the change in the apparent Gibbs free energy of adsorption as a function of coverage, Figure 2b, can be used to evaluate the isosteric heats of adsorption, e.g.,

$$q_{st}^H = - \frac{\partial(\Delta G_{H_{\text{UPD}}} / T)_0}{\partial T^{-1}} \quad (4)$$

As shown in Figure 2c, the change in the apparent enthalpy of adsorption as a function of coverage is linear. A fundamental measure of interest for the Pt(111)- $H_{\text{upd}}$  system is the Pt- $H_{\text{ad}}$  bond energy at the electrochemical interface. The absolute value of the Pt- $H_{\text{upd}}$  bond energy on Pt can be obtained from the heat of adsorption ( $q_{st}^H = -\Delta H_{H_{\text{UPD}}}$ ) through the relation

$$2E_{\text{Pt-H}} = |\Delta H_{ad}| + E_{diss} \quad (5)$$

where  $E_{\text{diss}}$  is the dissociation energy of  $H_2$ , 432 kJ/mol. It can be seen that the Pt-H bond energy ( $E_{\text{Pt-H}}$ ) varies from about 240-250 kJ/mol depending on the specific adsorption site and coverage. The resulting values ( $\Theta = 0$ ) of  $q_{st}^H = -\Delta H_{H_{\text{UPD}}}$ ,  $\Delta S_{H_{\text{UPD}}}$ ,  $\Delta G_{H_{\text{UPD}}}^0$  and  $f$ , and finally the  $E_{M-H}$  bond energies obtained for Pt(111) in alkaline solution are summarized in Table 1. The values are virtually identical *independent of the anion or the pH of solution* [28]. Note that, the energetics of Pt(111)- $H_{\text{upd}}$  follows the UHV-type of

linear decrease with  $\Theta_{H_{upd}}$ , reflecting repulsive lateral interaction in the  $H_{upd}$  adlayer and a weak (associative) adsorption of water onto the Pt surface.

The reversible adsorption of oxygenated species on Pt(hkl) (symbolized hereafter as  $OH_{ad}$ ) is more complex than  $H_{upd}$  adsorption [28]. The formation of the  $OH_{ad}$  layer in alkaline solution is just  $OH^-$  adsorption with charge transfer,



while in acid solution, the  $OH_{ad}$  adsorption proceeds according to



Because of the close coupling of  $OH_{ad}$  adsorption with  $H_{upd}$  (alkaline solutions) and anions (acid solutions) adsorption on Pt(100) and Pt(110), the thermodynamic state functions for the Pt- $OH_{ad}$  system can only be evaluated from the reversible formation of the  $OH_{ad}$  layer on Pt(111) in alkaline solution [28]. From the measured isosteric heat of adsorption of  $OH_{ad}$  (*ca.*  $\approx 200$  kJ/mol) the Pt(111)- $OH_{ad}$  bond energy in the so-called butterfly potential region ( $0.6 < E < 0.8$  V) was estimated to be  $\approx 136$  kJ/mol [28]. Although there is no true thermodynamic information about the Pt- $OH_{ad}$  bond strength at the Pt(110) and Pt(100) interfaces, these two surfaces appear to have bond energies that are at least 50-70 kJ/mol higher than on Pt(111). As a result, the reversible adsorption of  $OH_{ad}$  on these two surfaces is observed at very negative potentials (Figure 1). A careful inspection of voltammograms indicates that the adsorption of  $OH_{ad}$  on Pt(110) and Pt(100) may even start in the  $H_{upd}$  potential region. As shown in section 4.2.3, there are some indications that on the Pt(111) surface  $OH_{ad}$  is also present in the  $H_{upd}$  potential region. For  $OH_{ad}$  co-adsorbed with  $H_{upd}$  the Pt(111)- $OH_{ad}$  bond energy was calculated to be *ca.* 205 kJ/mol. An obvious question is why  $OH_{ad}$  does not react with co-adsorbed  $H_{upd}$  as it does in gas phase catalysis? The answer may be because at the Pt-solution interface the integrity of co-adsorbed  $H_{upd}$  and  $OH_{ad}$  is preserved through interaction with water molecules which are present in the inner part of the double layer. Notice that in his review article on hydrogen adsorption, Christmann [26] pointed out that although the initial (zero coverage) heat of adsorption on Pt(111) is the same at the solid-liquid and solid-gas interfaces, the change in heat of adsorption with coverage is very different.



This difference in  $H_{\text{upd}}-H_{\text{upd}}$  interaction energetics is attributed to the effect of water in the inner layer. An alternative answer may be that the negative value of the entropy of hydrogen adsorption (in Table 1 ca.  $\Delta S_{H_{\text{upd}}}^0 = -60 \text{ J/Kmol}$ ), characteristic for immobile adsorption of  $H_{\text{upd}}$  [35], may give rise to loss of 2D mobility, hence the reduced reactivity of an essentially fixed matrix of  $H_{\text{upd}}$  on Pt.

In acid solutions the adsorption of  $H_{\text{upd}}$  and  $\text{OH}_{\text{ad}}$  is always in competition with anions from supporting electrolytes. This competitive adsorption has an important, and generally adverse, effect on the adsorption of  $H_{\text{upd}}$ ,  $\text{OH}_{\text{ad}}$ , oxide formation and the formation of active intermediates. Of particular interest are chemisorbed (also called contact adsorbed or specifically adsorbed) anions, whose adsorption is controlled by both electronic and chemical forces. As recently summarized in reference [36], the nature of the Pt(hkl)-anion interaction is determined by two fundamental properties: (i) the strength of interaction, which for halide anions is controlled by the strength of anion hydration, e.g.,  $F^- < Cl^- < Br^- < I^-$ , and/or for polyatomic oxyanions is determined by the different degree of backdonation to the empty levels of the anion [37], e.g.,  $\text{ClO}_4^- < \text{HSO}_4^-$ ; (ii) the match between the symmetry of anions and the geometry of the surface, e.g. for tetrahedral (bi)sulfate anions the strength of interaction increases from Pt(100)  $\approx$  Pt(110) to Pt(111), while the spherical halides anions are more strongly adsorbed on (100) than on (111) sites. It is beyond the scope of this review to provide a comprehensive description of the Pt(hkl)-anion interaction. It is, however, important to emphasize that Pt(hkl) surfaces are *always* completely or partially covered with different kind of adsorbates between the HER and the onset of  $\text{O}_2$  evolution, and this has important consequences for the interpretation of the structure sensitivity of Pt single crystal surfaces.

#### 4.2.2.2 Structure sensitivity of the HER/HOR on Pt(hkl)

The need to understand the key structure relationships governing the electrocatalytic behavior of metal surfaces continues to motivate fundamental studies of surface processes at the solid-liquid interfaces. To this end, systematic variation of Pt surface crystallography has often been employed to delineate very important electrocatalytic trends. First reports for the HER at the Pt(hkl)-electrolyte interface

indicated that the kinetics of the HER in acid solutions is insensitive to the surface crystallography [38-41]. Recently, however, it was clearly demonstrated that the kinetics of the HER/HOR on Pt(hkl) vary with crystal face, depending on the electrolyte [36]. This structure sensitivity mainly arises due to structure sensitive adsorption of ions such as  $H_{\text{upd}}$  [42],  $OH_{\text{ad}}$  [42,43],  $HSO_{4,\text{ad}}$  [44],  $Cl_{\text{ad}}$  [45],  $Bi_{\text{ad}}$  [46], and  $Cu_{\text{upd}}$  [47]. Within the limited scope of this chapter, it will not be possible to review all of these results. Rather, using representative examples, the kind of information that can be used to improve our understandings of the role of local symmetry of platinum surface atoms in the HER/HOR will be summarized. For the purpose of demonstrating the effects of anions on the kinetics of the HER/HOR two sets of polarization curves are summarized in Figures 3 and 4. In acid solutions (Figure 3a and 3b), at low overpotentials ( $-0.2 < E < 0.2$  V) the order of activity is independent of temperature and increases in the sequence: Pt(111) < Pt(100) < Pt(110). It was found that at low overpotentials all three surfaces have a symmetrical  $\log i$  vs.  $E$  relationship [44], indicating that there is a single exchange current density for the hydrogen electrode reaction applicable to both anodic and cathodic processes. Using the values of  $i_0$ , assessed from the so-called “micropolarization” region over the temperature range 274-333K (inserts 3a and 3b), the apparent activation energies for the hydrogen reaction ( $\Delta H^\ddagger$ ) on Pt(hkl) in 0.05 M  $H_2SO_4$  can easily be determined from the Arrhenius plot, Figure 3c. Kinetic parameters for the HER/HOR on P(hkl) in 0.05 M  $H_2SO_4$  at different temperatures are summarized in Table 2. In contrast to acid solutions, in alkaline solutions the order of activity is strongly dependent on the temperature of electrolyte: while at 275 K the activity (qualitatively) increases in the sequence Pt(111) < Pt(100) << Pt(110) ( Figure 4a), at higher temperatures (Figure 4b) the Pt(100) surface is the least active, Pt(100) < Pt(111) << Pt(110). From the values of temperature dependent exchange current densities (inserts 4a and 4b), the apparent activation energies are determined (Figure 4c) and summarized in Table 2. Table 2 displays two important characteristics of the hydrogen reaction : (i) activation energies increase in the same order as the catalytic activity, and (ii) exchange current densities are markedly lower at higher pH of solution, producing activation energies in alkaline solutions that are doubled relative to the values obtained in acid solutions. From these

experimentally determined kinetic parameters, some of proposed models that can rationalize the structure-sensitive kinetics of the HER/HOR are discussed.

The postulated reaction steps of the HER/HOR in alkaline solution (8-10) are similar to those in acid solution (8'-10'), except that hydrogen is formed from H<sub>2</sub>O rather than from hydronium ions (H<sub>3</sub>O<sup>+</sup>). In the HOR, a slow Tafel step (Eqs. 8,8')



and/or Heyrovsky step (Eqs. 9,9')



is followed by a fast Volmer reaction (charge-transfer step (Eqs. 10,10')



Assuming that kinetic parameters are the same for the HER or the HOR close to the hydrogen reversible potential, then, the mechanism would be the same as that above for the HOR, *i.e.*, the fast charge-transfer step is followed by the Tafel and/or Heyrovski sequence. For the sake of discussion, the simplified kinetic equation for the HER/HOR can be expressed as:

$$i_0 = K(1 - \Theta_{ad}) \exp(-\Delta H^\# / RT) \quad (11)$$

in which K represents all structure insensitive parameters,  $\Theta_{ad} = \Theta_{H_{upd}} + \Theta_{H_{opd}} + \Theta_{OH_{ad}} + \Theta_{anions}$  is the surface coverage by adsorbed species, and  $\Delta H^\# = \Delta H^\#_{\Theta_{H_{opd}}=0} - \gamma r \Theta_{H_{opd}}$  is the measured activation energy in which  $\gamma r \Theta_{H_{opd}}$  represents the fraction of the decrease in the absolute value of the standard free energy of adsorption of active intermediates with increasing  $\Theta_{ad}$ . Schmidt et al., [43] used this equation to develop a model in which the formation of H<sub>opd</sub> (whose physical state is still unknown) on Pt(hkl) is determined by the structure sensitive adsorption of H<sub>upd</sub> and OH<sub>ad</sub>.

(a) *Effects of  $H_{\text{upd}}$ .* Considering that the kinetics of the HER/HOR are completely determined by the interaction of  $H_{\text{opd}}$  with the platinum surface atoms, the relationship between  $H_{\text{upd}}$  and  $H_{\text{opd}}$  is of fundamental importance in the electrocatalysis of the hydrogen reaction. As one can see below, the details are still unresolved, but there has been both progress and consolidation of ideas. For the purpose of distinguishing two different possible states of adsorbed hydrogen, one may employ a thermodynamic notation, referring to the  $H_{\text{upd}}$  state as a (relatively) “strongly” adsorbed state and  $H_{\text{opd}}$  as a “weakly” adsorbed state. The actual physical state of either  $H_{\text{upd}}$  or  $H_{\text{opd}}$  on a platinum electrode has been and continues to be the subject of intensive study. Closely following the Protopoff and Marcus proposition about the nature of  $H_{\text{upd}}$  and  $H_{\text{opd}}$  [8], it was proposed [36,42,44] that  $H_{\text{opd}}$  on Pt(hkl) is coupled to the strongly adsorbed state of  $H_{\text{upd}}$  by an as yet uncertain mechanism in which  $H_{\text{upd}}$  may have two modes of action on the  $H_{\text{opd}}$  state, thus on the kinetics of the HER/HOR on Pt(hkl):

(i)  $H_{\text{upd}}$  may block the adsorption of  $H_{\text{opd}}$  on the active Pt sites. This is consistent with the so-called *secondary structure sensitivity* observed in gas phase catalysis, where some secondary process in the reaction mechanism leads to site blocking. Thus, the HER/HOR is structure sensitive because during the reaction the number of exposed metal sites are different on each surface, so in Eq. 11  $i_0$  is proportional to the  $(1 - \Theta_{\text{Hupd}})$  term. In agreement with this simple model, the most active surface was found to be Pt(110), since by virtue of its unique surface geometry  $H_{\text{opd}}$  does not compete with  $H_{\text{upd}}$  for the same sites [42,44], as shown in Figure 4. Along the same lines, it was proposed that Pt(100) is more active than Pt(111) because the former surface provides more active centers for the formation of  $H_{\text{opd}}$ . These centers are either defect sites or sites created in the vicinity of the so-called subsurface  $H_{\text{upd}}$  [44].

(ii)  $H_{\text{upd}}$  may alter the energetics of  $H_{\text{opd}}$  [36,44], and, thus, in Eq. 11  $i_0$  is proportional to the  $\Delta H^\ddagger$  term. This “energetic” argument is in accord with the change of the apparent heat (enthalpy) of adsorption of  $H_{\text{opd}}$  with surface coverage, e.g.,  $\Delta H^\ddagger_{\Theta_{\text{Hupd}}} = \Delta H^\ddagger_{\Theta=0} - r\Theta_{\text{Hupd}}$ . In section 4.2.2.1 we learned that, independent of the pH, the heat of adsorption of  $H_{\text{opd}}$  on Pt(111) has a linear decrease with the surface coverage by  $H_{\text{upd}}$ , e.g., in Figure 2c from ca. 42 kJ/mol at  $\Theta_{\text{Hupd}} = 0$  to 24 kJ/mol at

$\Theta_{\text{H}_{\text{upd}}} = 0.66\text{ML}$ . Considering that the HER/HOR takes place on a *H<sub>upd</sub>-modified* platinum surface, the heat of adsorption of H<sub>opd</sub> on the “fully” H<sub>upd</sub>-covered Pt(111) surface must always be below 24 kJ/mol. It is noteworthy that this macroscopic picture still clearly separates the H<sub>upd</sub> state from the H<sub>opd</sub> state, *i.e.*, in the course of the reaction H<sub>upd</sub> and H<sub>opd</sub> occupy different kind of adsorption sites. Another possibility is that the adsorption of “extra” hydrogen (H<sub>opd</sub>) may cause H<sub>upd</sub> and H<sub>opd</sub> to adopt the same binding-site arrangement during the HER/HOR [43]. As a results, H<sub>upd</sub> and H<sub>opd</sub> become energetically indistinguishable on the surface ( $\Delta H_{\text{H}_{\text{upd}}}^0 = \Delta H_{\text{H}_{\text{opd}}}^0 < 24\text{kJ/mol}$ ), and thus, the H<sub>upd</sub> may act as *the* reactive intermediate in the HER/HOR. If this is the case, then this transformation from an unreactive H<sub>upd</sub> into a reactive H<sub>opd</sub> state may, in fact, be the structure sensitive process. This structure sensitivity is also reflected in the values of the apparent activation energies. In particular, due to both a low surface coverage of H<sub>upd</sub> (0.65 ML versus 0.82 ML) and a large repulsive interaction among the H<sub>upd</sub> atoms ( $r/RT \approx 11$  at 298 K), the activation barrier for this transition is much higher on Pt(111) than on Pt(110), see Tables 1 and 2. A review of the mechanism of the HER/HOR on Pt(hkl) with a different perspective from that given here can be found in the work of Conway and co-workers [48-51].

(b) *Effects of OH<sub>ad</sub>* The effect of OH<sub>ad</sub> on the HOR in the potential region where adsorption of OH<sub>ad</sub> is clearly visible in the voltammetry of Figure 1 ( $E > 0.4$  V) is unambiguous. That is, OH<sub>ad</sub> is acting as a site blocking inhibitor. This observation is not new and has been discussed at length, from the classical work of Breiter and co-workers [52] and Frumkin and co-workers [53] to very recent studies with Pt single crystal surfaces [43]. What was proposed recently, however, is that in the H<sub>upd</sub> potential region OH<sub>ad</sub> may act not only as a site blocking inhibitor but also as an energetic modifier, in the latter case affecting the energetics of the H<sub>upd</sub> (H<sub>opd</sub>) state through the H<sub>upd</sub>-OH<sub>ad</sub> interaction. This proposition is consistent with the results shown in Figure 4. For example, while at low temperatures the value of exchange current density is more than one order of magnitude different between the most active Pt(110) and the least active Pt(111), at higher temperatures this difference is less than factor of two, see Table 2. Furthermore, at 333 K Pt(111) is even more active than Pt(100) (Figure 4b), which then

results in the same order of absolute activity that Barber and Conway found in 0.5 M NaOH at 298 K [49]. Considering that the oxyphilicity of Pt(hkl) surfaces increases in the sequence Pt(111) << Pt(100) < Pt(110), a relatively small increase in the rate of the HER/HOR with temperature on Pt(110) and Pt(100) versus Pt(111) is then consistent with the temperature-enhanced (pH-enhanced in ref. [49]) adsorption of OH<sub>ad</sub> on these two surfaces. Note that, although Pt(110) is even more oxyphilic than Pt(100), the former is always the most active surface due to the uniquely high activity of the top rows of Pt atoms.

Inspection of Table 2 reveals that activation energies in alkaline solutions are more than doubled relative to the values obtained in acid solutions, producing exchange current densities on Pt(hkl) surfaces that are markedly lower at higher pH of solution. A similar pH effect for the HER/HOR kinetics on polycrystalline electrodes was reported some time ago by Osetrova and Bagotsky [54]. The authors suggested that the reaction followed a different path in alkaline solutions, *i.e.*, the formation of a H<sub>2</sub><sup>+</sup> intermediate rather than the dissociative adsorption of H<sub>2</sub>. Notice that, since the energetics of H<sub>upd</sub> formation in alkaline and acid solutions are very similar, section 2.2 and reference [28], the differences in the energetics of the formation of H<sub>opd</sub> states, from H<sub>2</sub>O in alkaline instead of H<sub>3</sub>O<sup>+</sup> in acid solution, appear to play a minor role in the pH-dependent kinetics of the HER/HOR. Bearing this in mind, Schmidt et al., have recently presented an argument that the puzzling pH-dependent kinetics of the HER/HOR may arise from the “pH-dependent” adsorption of OH<sub>ad</sub> in the H<sub>upd</sub> potential region and the contribution from  $\Theta_{\text{OHad}}$  to the  $(1-\Theta_{\text{ad}})$  and  $\Delta H^{\#}$  terms in Eq.11 [43]. The observation that OH<sub>ad</sub> species, whose real physical state is still as puzzling as the pH-kinetics of the hydrogen reaction on Pt, are present at the surface even close to the reversible potential has suggested some new experiments that may resolve the pH-dependent kinetics of the HER/HOR on Pt and other metal surfaces. Resolving this puzzle will go a long way toward developing a new catalyst for the hydrogen reaction.

#### 4.2.2.3 HER/HOR on Pt(hkl)-Pd metal films

During the last decade there has been a substantial growth in the understanding of the chemical and electronic properties of thin metal films supported on foreign metal

substrates [55,56]. The dissociative adsorption of H<sub>2</sub> on bulk Pd and Pd overlayers on the early transition metals occupies a special position in gas phase catalysis [57]. It was found that electron transfer from the surface into the  $\sigma^*$  antibonding orbital of the H<sub>2</sub> molecule plays a dominant role in the breaking of the H-H bond, thus lowering the activation energy associated with the process. Transition metals, such as pure Pd, are good electron donors, and dissociation of H<sub>2</sub> on this surface occurs readily at room temperature. In contrast, no dissociation of H<sub>2</sub> is observed on the Re(0001)-Pd, and Nb(110)-Pd systems because the charge transfer from the Pd overlayer to the substrate has induced a decrease in the electronic density of the Pd film [57]. The development of theoretical tools to describe and understand adsorption on thin metal films has been quite parallel to the experimental developments. For an overview of the key theoretical aspects of adsorption on ultrathin metal surfaces we refer readers to the review of Hammer and Norskov [58,59].

After the successful UHV studies, the adsorption and catalytic properties of pseudomorphic films supported on single crystal metal surfaces received considerable attention in the field of surface electrochemistry. As pointed out in a number of recent studies [60-65], catalytic activity and selectivity of many important electrochemical processes can be greatly enhanced by the addition of Pd to the primarily active metal. In this section, the current status of knowledge of the HER/HOR on well-characterized Pt(111)-Pd films is reviewed.

#### *4.2.2.4 Preparation and characterization of Pd metal films on Pt(hkl)*

For the electrochemical measurements, thin films of palladium can be prepared either in UHV by evaporation or in-situ by (electro)chemical methods. The electrodeposition method is fast and is particularly advantageous in deposition of palladium on platinum [60-66] and gold [67,68] single crystal surfaces. For fundamental studies, however, the electrochemical method of preparation has a major drawback of creating an unknown amount of deposit, as the process cannot be characterized by utilizing surface sensitive analytical probes (as in UHV). In UHV the most reliable method for determining the composition of the outermost layer of atoms is by low-energy-ion-scattering (LIES) using inert gas ions like helium or neon [69]. An example of UHV-prepared and LIES

characterized Pd films on Pt(111) and the corresponding cyclic voltammograms obtained in an electrochemical cell are summarized in Figure 5. As with electrochemically prepared Pd films [60,61,64], an increase in the surface coverage by Pd (peak at  $E/E_0 = 0.8$ ) led to a linear increase in the pseudocapacitance in the  $H_{\text{upd}}$  potential: from  $160 \mu\text{C}/\text{cm}^2$  on unmodified Pt(111) to  $320 \mu\text{C}/\text{cm}^2$  on Pt(111) covered with 1 ML of Pd.

The morphology and stability of Pd films on Pt(111) were examined by utilizing *in-situ* SXS [65] and FTIR [70] measurements. SXS studies demonstrated that electrochemically deposited films are pseudomorphic, whereby the Pd atoms occupied comencurate Pt sites such as to continue the ABC stacking of the Pt(111) substrate. These films were rather stable between the hydrogen evolution and the oxide formation potential region, showing no sign of the hydrogen absorption characteristic for bulk Pd and also observed for a 3D Pd island deposited on Pt(hkl) with  $\Theta_{\text{Pd}} > 1 \text{ ML}$  [71]. For increasing coverage beyond 1 ML of Pd, Pd deposition on Pt(111) follows the Stranski-Krasanov pseudomorphic mode of growth, e.g, three dimensional pseudomorphic crystalline islands of pure Pd begin to aggregate after *one* smooth monolayer of Pd is formed on the Pt substrate [72]. FTIR characterization of Pt(111)- $\text{CO}_{\text{ad}}$  modified with  $0 < \Theta_{\text{Pd}} < 1 \text{ ML}$  was used as an indirect method to establish whether Pd forms 2D islands or Pd atoms disperse on the surface much more randomly, as seen for the deposition of Bi on transition metals [73]. If the Pd adlayer coalesces into islands then one expects to see separate stretching frequencies corresponding to  $\text{CO}_{\text{ad}}$  on the Pd island and on the Pt substrate. On the other hand, if Pt and Pd are atomically mixed then a single vibrational CO band with frequency between those of the pure metals should be seen. These kind of effects have previously been observed in selected experiments by Friedrich et al for Pt-Ru alloys and Ru electrodeposited on Pt(111) systems [74] and for Pd and Rh monolayers on Pt(111) and Pt(100) [66]. Representative CO stretching frequencies on Pt(111) modified with 0.5 ML of Pd are shown in Figure 6b. As a reference, FTIR spectra for CO on Pt(111) and Pt(111)-1 ML Pd in KOH are also included in Figure 6a and 6c, respectively. For Pt(111), characteristic three-fold hollow C-O stretching bands, near  $2070 \text{ cm}^{-1}$  and atop C-O stretching bands near  $1780 \text{ cm}^{-1}$  predominate in the spectra obtained at potentials below 0.50 V [75,76,77,78]. For Pt(111)-1ML Pd, the observed single C-O stretching band near  $1870 \text{ cm}^{-1}$  can be assigned to bridge bonded  $\text{CO}_{\text{ad}}$



[66,70,79,80]. The appearance of three different C-O stretching bands, near  $1730\text{ cm}^{-1}$ ,  $1870\text{ cm}^{-1}$  and  $2035\text{ cm}^{-1}$  in the FTIR spectra of the Pt(111)-0.5 ML Pd system implies that Pd atoms cluster into islands and that Pt and Pd behave according to their surface chemistry. From these results, one would expect a gradual change in the catalytic properties of Pt(111)- $\Theta_{\text{Pd}}$  electrodes, from those characteristic of pure Pt(111) to those which are characteristic for Pt(111) covered with 1 ML of Pd. In the subsequent section it is shown that is, in fact, the case for the HER/HOR.

#### 4.2.2.4.1 *Kinetics of the HER/HOR on Pt(111) modified with Pd films*

For the purpose of demonstrating the effects of Pd atoms on the catalytic properties of Pt(111) two sets of polarization curves are summarized: the HER/HOR in acid solution in Figure 7, and the HER/HOR in alkaline solution in Figure 8. The HER/HOR on the Pt(111) modified by Pd show, depending on the surface coverage by Pd atoms, from minor enhancement in acid solution ( $\Theta_{\text{Pd}} \leq 1\text{ML}$ ) to strong activation in alkaline solution ( $\Theta_{\text{Pd}} \leq 1\text{ML}$ ) or deactivation in both electrolytes ( $\Theta_{\text{Pd}} > 1\text{ML}$ ). Figure 9 reveals that the general form of  $i$  vs.  $\Theta_{\text{Pd}}$  relationship has a volcano shape, with the maximum catalytic activity exhibited by the Pt(111) surface modified with 1 ML of Pd. From Figures 7 and 8, the unique catalytic activity of the 2D Pd layer is less obvious in acid than in alkaline solution, presumably due to the very fast kinetics of the HER/HOR on Pt in the former solution. Although the enhancement in acid solution is rather small, it is real, as indicated by an decrease in activation energy from 18 kJ/mol on an unmodified surface to 9 kJ/mol on Pt(111) covered with 1 ML of Pd. The activation energy on the Pt(111)-Pd electrode in alkaline solution is also a half of the value obtained for Pt(111), i.e., decreases from 40 kJ/mol on Pt(111) to 20 kJ/mol on Pt(111)-1 ML Pd. One way to understand the HER/HOR on Pt(111)-Pd surfaces is to find the link between  $i_0$  and the  $(1-\Theta_{\text{ad}})$  and/or  $\Delta H^\ddagger$  terms in Eq. 11.

Closely following the discussion for the HER/HOR on Pt(hkl) in section 2.2.2.2, the key to resolving the activity of the Pt(111)-Pd surfaces for the HER/HOR in the vicinity of the Nernst potential is to be found in understanding the nature of  $\text{H}_{\text{upd}}$  and how this state may effect the formation of  $\text{H}_{\text{opd}}$  in Eqs (8-10). Recall that, due to the strong interaction between Pd atoms and hydrogen, a full monolayer of  $\text{H}_{\text{upd}}$  is deposited on a

pseudomorphic Pd monolayer in both acid [64] and alkaline [70] solutions. Notice also that because of close coupling of anions (e.g. (bi)sulfate and halides in acid solutions and OH in alkaline solutions) and  $H_{\text{upd}}$  adsorption on Pd atoms, the determination of Pd- $H_{\text{upd}}$  energetics on this surface is problematic in both acid and alkaline solutions. The fact that on the Pt(111)-Pd surface a full monolayer of adsorbed  $H_{\text{upd}}$  can be formed, however, suggests that the Pd- $H_{\text{upd}}$  interaction is stronger than Pt- $H_{\text{upd}}$ . Consequently, some amount of  $H_{\text{upd}}$  might sit in deeper potential wells of the three-fold hollow sites, and thus be more in the surface than on the surface. Similarly to the argument used for Pt(100) in section 2.2.2.2, the HER/HOR may occur on a geometrically homogeneous Pt(111)-Pd surface fully covered by  $H_{\text{upd}}$  only if some amount of the  $H_{\text{upd}}$  is in the subsurface state, allowing adsorption of  $H_{\text{opd}}$  on the adjacent free Pd top-sites. An alternative explanation may be that the hypothetical transition from an unreactive  $H_{\text{upd}}$  layer into a reactive  $H_{\text{opd}}$  layer is enhanced on Pt(111)-Pd compared to unmodified Pt(111). This supposition is consistent with a high surface coverage of  $H_{\text{upd}}$  (1 ML versus 0.66 ML) and a small repulsive interaction between the  $H_{\text{upd}}$  atoms ( $r/RT < 11$  at 298 K) on Pd sites. However, when the Pd deposit exceeds 1 ML then the catalytic activity is linearly decreasing (Figure 9), so a surface covered by 3 ML of Pd becomes even less active than unmodified Pt(111). To explain the change in reactivity, Arenz et al. postulated a possible change in the H binding energy on Pt(111)-Pd surface induced by the *absorption* of hydrogen into the 3D Pd bulk phase (see model in Figure 9) [81]. As with Pt(111)-Pd, the hydrogen reaction on Pt(100)-Pd is optimized on 2D Pd islands ( $\Theta_{\text{Pd}} \approx 0.85$  ML) which are formed just before a 3D growth [71]. We can conclude, therefore, that there is apparent correlation between the rate of the HER/HOR and the surface coverage by Pd: Pt(111) and Pt(100) modified with ca. 1 ML of Pd having an unique catalytic activity for the hydrogen reaction.

### 4.2.3 Surface structure and kinetics of CO oxidation and H<sub>2</sub>/CO mixtures oxidation on Pt(hkl) and Pt(hkl) bimetallic surfaces

As in electrocatalysis of the HER/HOR, the ultimate challenge in electrocatalysis of CO is to relate the microscopic details of adsorbed states of intermediates to the macroscopic measurement of kinetic rates and thermodynamic state functions. Unfortunately, in the case of surface chemistry of CO on Pt(*hkl*) surfaces, this approach has an intrinsic difficulty. Given that CO adsorption on Pt(*hkl*) at near ambient temperature is an irreversible process, and due to the narrow temperature range available in aqueous solutions, the heat of adsorption of CO cannot be determined at Pt electrodes. One can use, however, the values of thermodynamic functions which are obtained from UHV measurements and test them in the electrochemical system for consistency. The second approach is to use computational methods which can give direct information on the binding energetics of CO on metal surfaces [82-84]. This computational approach provide invaluable information to compliment and correctly interpret experimental data. Closely following UHV terminology, it was proposed that energetically two forms of CO<sub>ad</sub> species can be distinguished on Pt(*hkl*) in an electrochemical environment [85]: (i) CO<sub>ad</sub> with a low heat of adsorption ( $\approx 65 \pm 15$  kJ/mol at saturation ) which is oxidized in the so-called the pre-ignition potential region is characterized as the “weakly adsorbed” state,  $CO_{ad}^w$ , and (ii) CO<sub>ad</sub> with a relatively high enthalpy of adsorption which is oxidized in the ignition potential region ( $\approx 150 \pm 15$  kJ/mol at low coverages ) is characterized as the “strongly adsorbed” state,  $CO_{ad}^s$ . These concepts for CO<sub>ad</sub> energetics, and the transition from the  $CO_{ad}^w$  state into the  $CO_{ad}^s$  state, are the keys to understanding the relation between reactivity and interfacial structures of CO<sub>ad</sub> on Pt(*hkl*) and Pt-bimetallic surfaces.

#### 4.2.3.1 Structures of CO<sub>ad</sub> on Pt(111)

Resent developments of in-situ techniques have provided very important information about local structures and phase transitions within ordered CO<sub>ad</sub> adlayers at the Pt(*hkl*)-electrolyte interfaces. The presentation here is restricted to the adsorption of CO on Pt(111); further details (including experimental procedures, interaction of CO with the

other two low index platinum single crystal surfaces, and CO induced relaxation of Pt surface atoms) can be found in a recent review article [36]. In early studies, STM gained a certain prominence among the other methods to characterize *in-situ* adsorbed CO at the Pt(111)-liquid interface. A compressed carbon monoxide adlayer on Pt(111) in aqueous acidic solution was observed by STM [86]. Depending on the CO<sub>ad</sub> surface coverage and the applied potential four different structures were found, including the  $(\sqrt{3}x\sqrt{3})R30^0$  structure which is observed in *ex-situ* RHEED measurements [87]. Key STM work along with *in-situ* FTIR was done by Villegas and Weaver [88,89], who observed a hexagonal closed packed (2 x 2)-3CO adlayer structure in the H<sub>upd</sub> potential region with a CO<sub>ad</sub> coverage of  $\Theta_{CO} = 0.75$  ML. At more positive potentials a markedly different adlayer arrangement was formed, having a  $(\sqrt{19}x\sqrt{19})R23.4^0 - 13CO$  unit cell with  $\Theta_{CO} = 13/19$ . Very recently, the Pt(111)-CO<sub>ad</sub> system was studied in detail by a combination of SXS [85,90] with FTIR and SFG spectroscopes [91]. These studies demonstrated that, although the nature and adsorption site occupancy of CO<sub>ad</sub> are strongly dependent on the applied potential, the mechanism for CO<sub>ad</sub> oxidation on Pt(111) is independent of electrode potential; *e.g.* CO<sub>ad</sub> reacts with oxygen-containing species through either a non-competitive or competitive Langmuir-Hinshelwood (L-H) type reaction to form CO<sub>2</sub> [85]. The physical state of oxygen-containing species is still uncertain (bulk H<sub>2</sub>O, adsorbed H<sub>2</sub>O or adsorbed OH) [92]. If CO<sub>ad</sub> is oxidized by OH<sub>ad</sub>, the latter species resulting from oxidative water decomposition in acid solution or from OH<sup>-</sup> discharge in alkaline solution [28,85] then the reaction takes place according to Eq. 12[28]:



The interesting point is that the kinetics of Eq. 12 as well as the structure of CO<sub>ad</sub> on the Pt(111) surface are not governed only by the surface concentration of CO<sub>ad</sub> and OH<sub>ad</sub> species, but are strongly affected by a delicate balance between the coverage of CO<sub>ad</sub>, OH<sub>ad</sub> and *anions* from supporting electrolytes [28,85]. In what follows we describe the Pt(111)-CO<sub>ad</sub> system in some detail by means of *in-situ* SXS and FTIR techniques,

emphasizing the role of anions in controlling the ordering, stability, and reactivity of the CO<sub>ad</sub> adlayer, Figures 10-12.

In perchloric acid solution, Figure 10, Lucas et al [90] have found that while holding the potential at 0.05 V and with a continuous supply of CO to the x-ray cell, a diffraction pattern consistent with a p(2 x 2) symmetry was observed, which is in a good agreement with previous STM results [89]. With a constant overpressure of CO in the x-ray cell, the SXS experiments revealed a *reversible* order-disorder transition of the p(2 x 2)-3CO structure. Although a careful search was made to find diffraction peaks due to STM observed CO<sub>ad</sub> structures, such superlattice peaks were not found in SXS measurements at any partial pressure of CO and at any surface coverage by CO. It was concluded, therefore, that the p(2 x 2)-3CO structure is the only structure present with *long-range order* [90]. A rocking scan through the (½, ½, 0.2) position is shown in Figure 13b together with the fit of a Lorentzian lineshape (solid line) to the data. From the width of this peak and from the result of similar fits to other p(2 x 2) reflections a coherent domain size in the range of 80-120 Å was deduced [85,90,93]. The derived structural model is shown schematically in Figure 11, which consists of three CO molecules per p(2 x 2) unit cell. As shown in Figures 10-13, the stability/domain size of this structure increases from KOH (*ca.* 30 Å between 0.05 < E < 0.3 V), to HClO<sub>4</sub> (*ca.* 140 Å between 0.05 < E < 0.6 V) to HClO<sub>4</sub> + Br<sup>-</sup> (*ca.* 350 Å between 0.05 < E < 0.8 V). It is important to note, however, that besides the symmetry of the ordered CO structure, SXS measurements were unable to provide information about Pt adsorption sites in the unit cell. As mentioned above, this information is obtained from FTIR measurements.

In the FTIR measurements, Figures 10-12, characteristic C-O stretching bands near 2070 and near 1780 cm, corresponding to atop and three-fold hollow CO respectively [75-78,93], predominate in the spectra obtained at lower potentials. At higher potentials, the three-fold hollow band is replaced by a new C-O stretching band at *ca.* 1840 cm<sup>-1</sup> that can be related to the presence of bridge-bonded CO. This transition in the binding-sites occupancies is strongly dependent on the nature of anions present in supporting electrolytes, e.g., the transition from three-fold hollow to bridge-bonded sites shifts towards more positive potentials going from KOH (E = 0.2 V) to HClO<sub>4</sub> (E = 0.6 V) to HClO<sub>4</sub> + Br<sup>-</sup> (E = 0.9 V) solution. Plots for the integrated intensity of the observed C-O

stretching bands along with  $\text{CO}_2$  ( $\text{CO}_3^{2-}$  in alkaline electrolytes) as a function of the electrode potential are also summarized in Figures 10-12. Comparison of the potential dependent intensity changes for the three-fold and bridge CO bands with the SXS [93,94] data reveals that the three-fold hollow band is related to the  $p(2 \times 2)$ -3CO structure whereas the loss of this ordered structure is reflected by the appearance of the bridge-bonded CO band.

Another point that can be clarified from the *in-situ* SXS and FTIR experiments is that of the relation between the loss of the  $p(2 \times 2)$  structure and the onset of CO oxidation. On the basis of SXS and voltammetric data it was found that the disordering transition is governed by electrooxidation of a relatively small amount of  $\text{CO}_{\text{ad}}$ , *ca.* 15% [85]. This can be confirmed from Figure 10a, which provides a quantitative measure of  $\text{CO}_2$  formation from the asymmetric O-C-O stretch at  $2343 \text{ cm}^{-1}$ . Compared with Figure 10-12,  $\text{CO}_2$  ( $\text{CO}_3^{2-}$ ) production occurs simultaneously with the binding site occupancy change, indicating that structural transformation in the  $\text{CO}_{\text{ad}}$  layer is triggered by oxidative removal of  $\text{CO}_{\text{ad}}$  [93]. Interestingly, the  $\text{CO}_2$  ( $\text{CO}_3^{2-}$ ) plot shows two (positive) slopes: the low slope corresponds to the pre-ignition region where disappearance of the three-fold hollow sites is observed in Figures 10-12, and the high slope that is related to the oxidation of atop and bridge  $\text{CO}_{\text{ad}}$  in the ignition potential region. The point of inflection in the  $\text{CO}_2$  ( $\text{CO}_3^{2-}$ ) slope may correspond to the “ignition potential”, e.g., the potential for the steep onset of  $\text{CO}_2$  ( $\text{CO}_3^{2-}$ ) production [93]. Notice that the ignition potential is the electrochemical analog of ignition temperature for the gas phase oxidation of CO. Therefore, linking macroscopic and microscopic characterization of the Pt(111)-CO system, the macroscopic terminology of  $\text{CO}_{\text{ad}}^w$  may correspond microscopically to a saturated  $\text{CO}_{\text{ad}}$  layer consisting of three CO molecules per  $p(2 \times 2)$  unit cell located in atop and three-fold hollow sites. Figures 10-12 show that oxidation of  $\text{CO}_{\text{ad}}$  in the three-fold hollow sites and relaxation of the remaining  $\text{CO}_{\text{ad}}$  into bridge sites and atop sites disrupts the long-range ordering in the remaining adlayer, as the Bragg peak intensity for the  $p(2 \times 2)$ -3CO structure decreases rapidly in this potential region. The “relaxed”  $\text{CO}_{\text{ad}}$  adlayer (characterized microscopically) with substantial alternation in binding site geometry from predominantly three-fold hollow to bridge sites can be

linked macroscopically to the strongly adsorbed state of  $\text{CO}_{\text{ad}}$  that is oxidized in the ignition potential region. The factors which are determining the kinetics of this reaction are summarized below.

#### 4.2.3.2 Kinetics of $\text{CO}_b$ oxidation on Pt(111)

The role of anions in the kinetics of  $\text{CO}_b$  electrooxidation can be seen by comparing the polarization curves for  $\text{CO}_b$  oxidation on Pt(111) in different electrolytes. Figure 14 shows that the activity of Pt(111) increases in the sequence:  $\text{Br}^- \ll \text{HClO}_4 \ll \text{NaOH}$ . In the latter case, the onset of the pre-ignition region is in what is generally considered to be the  $\text{H}_{\text{upd}}$  potential region (!). If the L-H mechanism is operative, the catalytic activity in the  $\text{H}_{\text{upd}}$  potential region implies that in alkaline solution  $\text{OH}_{\text{ad}}$  is adsorbed even at potentials below *ca.* 0.25 V (vs. RHE). In reference [28], it was proposed that adsorption of  $\text{OH}_{\text{ad}}$  in the  $\text{H}_{\text{upd}}$  potential region occurs at the defect/step sites on the Pt(111) surface. The low defect density on the Pt(111) surface explains the relatively low rate of reaction achieved in this potential region. On the Pt(100) surface, where the defect density is high due to the lifting of the reconstruction, the activity in the same potential region is much higher than on Pt(111), as illustrated in the insert of Figure 14. The explanation, therefore, for the remarkable effect of pH on the rate of  $\text{CO}_b$  oxidation on Pt(hkl) is the “pH dependent” adsorption of  $\text{OH}_{\text{ad}}$  at defect/step sites. In acid solution at low overpotentials  $\text{OH}_{\text{ad}}$  is most likely excluded from active sites, *e.g.*, the dipole moment at defect/step sites is intrinsically attractive to anions [28]. The fact that in solution containing bromide the ignition potential is shifted *ca.* 0.6 V positively from that observed in alkaline solution implies that  $\text{Br}^-$  can indeed effectively suppress the adsorption of  $\text{OH}_{\text{ad}}$ . It is obvious, therefore, that both  $\text{CO}_{\text{ad}}$  and  $\text{OH}_{\text{ad}}$  must be present on the surface for the reaction to proceed at some reasonable rate.

#### 4.2.3.3 $\text{H}_2/\text{CO}$ mixture oxidation on Pt(111)

The discussion so far has been restricted to the kinetics and structure sensitivity of pure  $\text{H}_2$  and CO gasses at the Pt(hkl)-liquid interface. Since, from a practical standpoint the understanding of the kinetics of  $\text{H}_2/\text{CO}$  mixtures is of much greater importance for the development of fuel cells running on either industrial hydrogen or hydrogen feed streams derived from carbon based fuels, the following discussion will be concentrated

on the kinetics of the HOR in the presence of a trace level of CO. In general, the electrooxidation of H<sub>2</sub>/CO mixtures on Pt is a very complicated reaction which includes (non)competitive adsorption and desorption steps of electroactive species (H<sub>2</sub>, CO<sub>b</sub>), reaction products (H<sup>+</sup>, CO<sub>2</sub>), and reactive (H<sub>opd</sub>, CO<sub>ad</sub>, OH<sub>ad</sub>) and non-reactive (H<sub>upd</sub>, anions, oxide) intermediates. It is, therefore, not surprising that the reaction mechanism of H<sub>2</sub>/CO mixtures in the pre-ignition potential region is still controversial. There have been discussions in the literature as to whether the H<sub>2</sub> oxidation reaction proceeds concurrently with the oxidation of CO<sub>ad,w</sub> or the rate of the HOR is determined by the CO<sub>ad</sub> adsorption/desorption equilibrium coverage ( $\Theta_{\text{COad}}$ ) in the absence of CO oxidation. Distinction between these two reaction mechanisms is very complicated to achieve, mainly because both of them assume that the resulting decrease in  $\Theta_{\text{COad}}$  is equivalent to an increase of the vacancies in the CO<sub>ad</sub> layer which, in the case of H<sub>2</sub>/CO mixtures, will produce a large rise of the H<sub>2</sub> electrooxidation rate. Nevertheless, under specific experimental conditions, e.g., partial pressures of CO greater than 0.01 atm., it has been found that the oxidation of CO<sub>ad</sub> is a necessary prerequisite for the HOR to proceed in the pre-ignition potential region. The first evidence that the HOR in the pre-ignition region occurs concurrently with the removal of CO<sub>ad</sub> was obtained by monitoring the H<sub>2</sub> oxidation current on the Pt(111) surface completely covered by CO<sub>ad</sub> ( $\Theta_{\text{CO}} = 0.75 \text{ ML}$ ) [85]. For example, Figure 15 shows that on the platinum surface which is completely covered with pre-adsorbed CO<sub>ad</sub> the electrooxidation of H<sub>2</sub> (1 atm) in CO-free solution (dotted curve) coincides with the potential at which the oxidative removal of CO<sub>ad</sub><sup>w</sup> is observed in stripping voltammetry (solid curve). Therefore, H<sub>2</sub> oxidation occurs *concurrently* with the oxidative removal of the CO<sub>ad</sub><sup>w</sup> state. The correlation between the rate of the HOR and the stripping charge for CO<sub>ad</sub> oxidation on the Pt(111) surface (Figure 16) demonstrates that a diffusion limiting current for the HOR is observed after removal of about 30% of the total amount of pre-adsorbed CO<sub>ad</sub>. The oxidation of H<sub>2</sub> on CO-poisoned Pt(hkl) surfaces is a strongly structure sensitive reaction, the rate being ca. 50 times higher on the (100) surface than on Pt(111), in agreement with the model that at low potentials oxygenated species are preferentially adsorbed at the defect/step sites [95]. From a practical standpoint, the structure sensitivity is not so interesting, since at any



realistic level of CO (> 10 ppm CO) and temperature the pure Pt surface is highly poisoned with CO<sub>ad</sub> and the electrode polarization is impractically large. It is, however, still of fundamental importance to understand the structure sensitivity of this reaction in order to understand the properties of Pt-based alloy CO-tolerant catalysts, as discussed in section 3.4.

Additional evidence that the kinetics of the HOR in the pre-ignition potential region is controlled by the oxidation of the adsorbed CO could also be found in selective experiments for the electrooxidation of CO<sub>b</sub>/Ar mixtures and CO<sub>b</sub>/H<sub>2</sub> mixtures. As shown in Figure 17, the continuous supply of CO<sub>b</sub>, even 2%, leads to *re-poisoning* of the surface, and consequently to inhibition of the HOR. If the partial pressure of CO is reduced from 1 atm. to 0.02 atm. by means of a CO/Ar mixture, the "ignition" potential of CO oxidation shifts *negatively* versus pure CO ( $\approx 0.1$  V in Figure 17b), producing a negative reaction order for the oxidation of CO<sub>b</sub> on Pt at  $E > 0.85$  V [85], as observed on polycrystalline Pt. A simple L-H model for the competitive adsorption of CO and H<sub>2</sub>O can account for this negative reaction order. In contrast to the "ignition" potential, in the pre-ignition potential region a reduced partial pressure of CO lead to a decrease in the rate of CO<sub>b</sub> electrooxidation, consistent with a *positive* reaction order for the CO<sub>b</sub> oxidation with respect to partial pressure of CO [95]. It is important to note that the electrooxidation of H<sub>2</sub> is strongly deactivated in the presence of 2% CO, so the transition from an inactive, e.g. CO-poisoned, surface to a highly active surface occurs in a very narrow potential band, and is clearly related to the concomitant CO oxidation reaction in H<sub>2</sub> free solution. Although the H<sub>2</sub> oxidation current is quite low in the pre-ignition region, this rate could be practically useful if the pre-ignition region could be shifted much closer to 0 V. The surprising thing is that in fact this can actually be done, by alloying Pt with Ru [96-99], Mo [100-103], Sn [104,105] and other metals [106-108].

#### 4.2.3.4 CO and H<sub>2</sub>/CO mixtures oxidation at Pt-bimetallic surfaces

In general, the significant catalytic enhancement produced by alloying Pt with a second element can be ascribed to one or more of the following: *bifunctional* effects where the second component provides one of the necessary reactants; *ligand* (electronic) effects where the second component (promoter) alters the electronic properties of

catalytically active metal; and *ensemble* (morphological) effects where the dilution of the active component with the catalytically inert metal changes the distribution of active sites, thereby opening different reaction pathways. The concept of bifunctional catalysis was initially established in the field of gas-phase catalysis [109] and predates the appearance of the concept in the electrochemical community by about two decades. The bifunctional model in electrocatalysis was introduced some time ago by Watanabe and Motoo for the oxidation of bulk (dissolved)  $\text{CO}_b$  on a Pt surface modified by electrodeposited Ru [110]. This concept is fairly straightforward: modify the surface of Pt with an admetal that is more oxyphilic than Pt and shift the potential for OH formation (on the adatom site) negatively by (hopefully) a few tenths of a volt. In contrast, information for the electronic effects in electrocatalysis of CO were sketchy because the direct information on the binding energy of  $\text{CO}_{\text{ad}}$  and  $\text{OH}_{\text{ad}}$  on the different Pt bimetallic surfaces were relatively difficult to extract from electrochemical measurements (see sections above). More recently, however, Shubina and Koper [84] and Liu and Norskov [83] used a computational approach in order to assess the quantum-chemical nature of the adsorption of CO and OH on a variety of bimetallic surfaces. These density functional theory (DFT) calculations have provided invaluable information to complement previous experimental studies related to  $\text{CO}_b$  oxidation on Pt-bimetallic surfaces [36]. For instance, the DFT study of the adsorption of CO and hydroxyl on PtRu alloys showed a clear trends towards a weakening of the CO bond to Pt when the surface/substrate became enriched in Ru, and a strengthening of the CO band to Ru when the surface/substrate became enriched in Pt [83,84,111]. The binding energy changes are electronic alloying effects (the ligand effect) that can be explained by the d band shift model of Hammer and Norskov [112]. As expected, the OH bond is stronger to Ru than is to on Pt (by about 1eV) and hence Ru does affect the CO oxidation rate by dissociating  $\text{H}_2\text{O}$  faster than Pt (the bifunctional effect). Clearly, DFT calculations for adsorption of CO and OH on Pt-Ru are in agreement with experimental findings that, although CO and OH *compete* for the same sites OH is preferentially adsorbed on the Ru sites, leading to both a negative reaction order with the respect to the concentration of  $\text{CO}_b$  [99] and to a *pseudo-bifunctional* mechanism. In the case of PtMo, the mixing of Pt by Mo leads to weakly adsorbed CO on both Pt and Mo sites( depending on the binding sites between –

0.56 to  $-1.06$  eV), and OH is strongly adsorbed only on Mo sites (with binding energy of  $-2.89$  eV) [84], confirming the experimental observation that Pt-Mo is a “true” bifunctional catalyst [102]. For the Pt-Sn system, DFT calculations showed that CO binds only to Pt (having the weakest binding energy of  $-1.41$  eV on atop Pt) and not to the Sn, whereas OH has an energetic preference for the Sn sites (with binding energy of  $-2.66$  eV) [84]. The latter finding is in variance with earlier semi-empirical cluster calculations by Anderson et al., which have shown that substitutional Sn atoms in a Pt cluster do not bind OH more strongly than Pt [113]. On the other hand, the former calculations are in agreement with the mechanism in which both the bifunctional effect and the ligand effect contribute to CO oxidation on Pt-Sn [104,105].

#### 4.2.3.4.1 *CO oxidation at Pt<sub>3</sub>Sn(hkl) surfaces*

Concentrating on both catalytic activity and structure sensitivity, Gasteiger et al demonstrated that : (i) the ignition potential for CO<sub>b</sub> electrooxidation on Pt<sub>3</sub>Sn(111) and Pt<sub>3</sub>Sn(110) single crystals in acid solution is dramatically reduced in comparison with Pt, e.g. by ca. 0.7V compared to pure Pt(111); (ii) the ignition potential for CO oxidation on the Pt<sub>3</sub>Sn(111) surface is 0.1 V lower than for the sputtered Pt<sub>3</sub>Sn(110) surface having (nearly) the same surface composition, demonstrating an unusually large structural effect created by the unique states of CO<sub>ad</sub> and OH<sub>ad</sub> at the Pt-Sn interface; (iii) the reaction order with the respect to the partial pressure of CO on Pt<sub>3</sub>Sn(hkl) alloys is positive, ca +0.25 for Pt<sub>3</sub>Sn(110) and ca. +0.5 for Pt<sub>3</sub>Sn(111). This positive reaction order would be consistent with the bifunctional mechanism, e.g. the ability of Sn to donate oxygenated species (again, symbolized hereafter as OH<sub>ad</sub>), which can then oxidatively remove CO<sub>ad</sub> from Pt [104,105],



Moreover, Gasteiger et al., have proposed that the uniquely high activity of Pt<sub>3</sub>Sn alloy surfaces, and the (111) surface in particular, is due to the formation of a “weakly adsorbed state of CO, CO<sub>ad</sub><sup>w</sup>. Although the formation of a CO<sub>ad</sub><sup>w</sup> state is a consequence of the strong intermetallic bonding between Pt and Sn atoms (the ligand effect), the actual physical state of CO<sub>ad</sub><sup>w</sup> was unknown. Recently it has been reported a detailed SXS/FTIR

study of the adsorption of CO at the Pt<sub>3</sub>Sn(hkl) surface. Representative results are summarized below.

As for the Pt(111)-CO<sub>ad</sub> system, the microscopic nature of CO<sub>ad</sub><sup>w</sup> on Pt<sub>3</sub>Sn(111) (UHV prepared and characterized) was recently established using the SXS/FTIR approach. SXS results revealed that, in contrast to Pt(111): no ordered structures of CO<sub>ad</sub> are formed on the Pt<sub>3</sub>Sn(111) surface and the expansion of Pt surface atoms upon the adsorption of CO on the Pt<sub>3</sub>Sn(111) surface (ca. 1.5%) is significantly smaller than the 4% expansion induced by the adsorption of CO on Pt(111). As discussed in reference [94], the difference in relaxation of the surface atoms may arise from the variation in the strength of the CO<sub>ad</sub>-substrate interaction, the CO<sub>ad</sub>-Pt<sub>3</sub>Sn(111) interaction being much weaker than CO<sub>ad</sub>-Pt(111) interaction. This may reflect that CO clustering as well as the energetics of CO<sub>ad</sub> can be affected by surrounding Sn atoms. This point is especially clear from FTIR data depicted in Figure 18. Neither a top/three-fold-hollow nor atop/bridge combination of CO<sub>ad</sub> binding sites, which are characteristic for Pt(111), are observed on Pt<sub>3</sub>Sn(111). Secondly, in contrast to the near invariant bandshape of atop CO<sub>ad</sub> on Pt(111) (Figure 10), changes in the band morphology (splitting of bands) and vibrational properties (increase in the frequency mode) of CO<sub>ad</sub> are clearly visible on the Pt<sub>3</sub>Sn(111) surface (Figure 18). The splitting of CO bands in FTIR measurements is commonly observed in UHV on the surface pre-covered by oxygen [114,115] or occasionally at the solid-liquid interfaces for more oxyphilic metals than Pt [79,116]. Based on these observations, and bearing in mind that at the Pt<sub>3</sub>Sn(111)-electrolyte interface CO<sub>ad</sub> is surrounded by oxidized Sn atoms, it was proposed that the splitting of the atop CO band may be caused by the presence of oxygenated species on the Sn atoms. Figure 18 shows that the Pt<sub>3</sub>Sn(111) surface has a preference for *atop* CO<sub>ad</sub>, e.g., a pair of bands centered at ca. 2090 cm<sup>-1</sup> and ca 2077 cm<sup>-1</sup> (at low potentials), are transformed into a single relatively broad peak centered at ca. 2077 (at higher potentials). These FTIR results are in disagreement with the DFT calculations, the latter showing that for CO adsorption on the Pt<sub>3</sub>Sn(111) surface the hollow hcp three-fold hollow site, with the Sn atom in the second layer, is preferred over atop site by ca. 0.41 eV. To explain this difference, Stamenkovic et al., suggested that in addition to electronic alloying effects

(the chemical shift introduced due to the chemical interaction between CO and Pt-Sn) the observed frequency shift could also be due to vibrational coupling between neighboring  $\text{CO}_{\text{ad}}$  and oxygenated species adsorbed *on* Sn atoms (through-space dipole-dipole coupling) [117]. The existence of a repulsive CO-O interaction and compression of  $\text{CO}_{\text{ad}}$  and  $\text{O}_{\text{ad}}$  islands on Pt surfaces are well established in UHV experiments and have been discussed independently by Engel and Ertl [118] and White [119]. Using the same arguments, Stamenkovic et al., suggested that the repulsive  $\text{CO}_{\text{ad}}\text{-OH}_{\text{ad}}$  interaction might account for may an increase in the  $\text{CO}_{\text{ad}}$  stretching frequency on  $\text{Pt}_3\text{Sn}(111)$  (Figure 18) relative to  $\text{Pt}(111)$  (Figure 10) [117]. Apparently, a final answer to this experimental observation has to await further investigations, perhaps by some theoretical calculations. Nevertheless, although there is generally no straightforward correlation between the C-O stretching frequency and binding energy [84], the higher frequency mode of  $\text{CO}_{\text{ad}}$  on  $\text{Pt}_3\text{Sn}(111)$  compared to  $\text{Pt}(111)$  may indicate the weaker CO binding to the former surface. Therefore, linking microscopic and macroscopic characterization of the  $\text{Pt}_3\text{Sn}(111)\text{-CO}_{\text{ad}}$  system, the macroscopic terminology of the weakly adsorbed  $\text{CO}_{\text{ad}}$  state (“crowded”  $\text{CO}_{\text{ad}}^{\text{w}}$  adlayer) may correspond microscopically to disordered compressed  $\text{CO}_{\text{ad}}$  layer consisting  $\text{CO}_{\text{ad}}$  molecules terminally bonded to Pt sites. Figure 18 shows that the onset potential for the oxidative removal of  $\text{CO}_{\text{ad}}^{\text{w}}$  ( $\text{CO}_2$  production) begins at 0.1 V, e.g., negative of the pseudocapacitance feature observed between  $0.3 < E < 0.5$  V in Figure 19. Until recently, the nature of this pseudocapacitance was unknown: i.e., it could be due to any number of processes, hydrogen adsorption, OH adsorption, or a Sn surface redox process. Very recently, FTIR spectroscopy showed that the adsorption of bisulfate anions takes place in this potential range [117], see Figure 19c. The single band at ca.  $1200\text{ cm}^{-1}$  can be assign to  $\text{SO}_3$  asymmetric stretching mode of bisulfate anions adsorbed *on*  $\text{Pt}(111)$  sites via three unprotonated oxygen atoms. Very similar spectra were recorded for the adsorption of bisulfate on  $\text{Pt}(111)$  in sulfuric acid solution [120-123] indicating that, in contrast to the  $\text{Pt-Sn-CO}_{\text{ad}}$  system, oxygenated species adsorbed on Sn have no effect on the active bisulfate IR bands. Returning to the  $\text{CO}_2$  production shown in Figure 18, we note that the time resolved  $\text{CO}_2$  production (not shown) indicated that in solution containing CO a small but continues production of  $\text{CO}_2$  takes place at

0.1 V. As discussed below, it turns out that this small activity is an important property for CO-tolerant catalysts.

#### 4.2.3.4.2 $H_2/CO$ oxidation at $Pt_3Sn(hkl)$ surfaces

Of the various possible  $H_2/CO$  compositions, the electrooxidation of  $H_2$  containing 0.1% and 2 % of CO on  $Pt_3Sn(111)$  is used here to provide a benchmark case. The main reason for studying the electrooxidation rates of CO and the  $CO/H_2$  mixtures was the envisaged technological use of Pt-Sn alloy catalysts as anode electrodes in PEM fuel cells using reformed methanol as the fuel. Gasteiger et al. have shown that the kinetics of  $H_2$  oxidation of 2 %  $CO/H_2$  mixtures follows the CO oxidation behavior of 2%  $CO/Ar$  mixtures [104], where  $H_2$  oxidation occurs *concurrently* with the oxidative removal of the  $CO_{ad}^w$  state. Based on this observation the reaction mechanism for oxidation of  $CO/H_2$  mixtures on  $Pt_3Sn(111)$  can be described as follows: Sn serves to nucleate  $OH_{ad}$  species at lower potentials compared to a pure Pt electrode, leading to the oxidative removal of  $CO_{ad}^w$  on nearby Pt sites and thus freeing Pt sites for the hydrogen oxidation reaction. This model suggests, therefore, that there is a contribution from both ligand (formation of  $CO_{ad}^w$ ) and bifunctional effects. While  $ad_{metal}$  may lead to this simple mechanism, the details of the reaction are very complex, with many factors contributing to the structure sensitive kinetics of  $H_2/CO$  oxidation on  $Pt_3Sn(hkl)$  surfaces. Figure 20 is shown to demonstrate that for two surfaces, having the same nominal surface composition of Sn (ca 20-25 at%), the onset potential for the oxidation of CO and  $CO/H_2$  mixtures on the (111) surface was shifted cathodically by 0.13 V relative to the (110) surface. Both the structure sensitivity and the high catalytic activity of the  $Pt_3Sn$  surface were attributed to the  $CO_{ad}^w$  state which is very reactive on the (111) surface. In conclusion, it appears that both the bifunctional effect and the ligand effect contribute to the influence of Sn on the CO oxidation rate and on  $H_2$  oxidation process in the presence of CO. Interestingly, although Pt-Sn is a better CO oxidation catalyst than Pt-Ru (at least above 0.2 V), the latter is used as a practical catalyst for the direct oxidation of syngas. The fact that one catalyst can be a good catalysts for CO oxidation but not an equally good CO-tolerant catalyst is not a particularly a surprising result. The relative inactivity of Pt-Sn at

technologically important potentials can be attributed to both a very low turn over frequency, defined as the number of complete reaction events per active sites per second, of  $CO_{ad}^w$  below 0.2 V (leading to a small number of Pt sites required for the adsorption of  $H_2$  molecules) as well as to an absence of  $H_2$  adsorption on Sn. In contrast to Sn, at elevated temperatures, Ru atoms become active for the dissociative adsorption of  $H_2$  and thus, although the turn over frequency of oxidative removal of  $CO_{ad}$  on Pt-Ru is as low as on Pt-Sn, the number of active sites for  $H_2$  adsorption is higher on the former surface. Different kinetic model for oxidation of the  $H_2/CO$  mixtures on Pt-Ru alloys has recently been developed by Liu and Norskov [83]. In the latter study, the DFT calculations were used to make a direct prediction of the effect of Ru on the performance of a Pt-Ru anode for the  $H_2$  oxidation in the presence of CO. The main conclusions of this work were that while for the CO oxidation process both ligand and bifunctional effects contribute to the enhanced kinetics on Pt-Ru, for the HOR process in the presence of small amounts of CO *only* the ligand effect is important. In particular, the Ru-induced weakening of the Pt- $CO_{ad}$  bond directly decreases the  $CO_{ad}$  coverage and hence increases the number of Pt site available for  $H_2$  oxidation. The Pt-Sn system discussed above shows, however, that even though the search for more CO tolerant Pt based catalysts should be focused towards alloys that bind CO more weakly than Pt (the ligand effect), it is also important that the alloying component should be active for CO oxidation (the bifunctional effect) and dissociative adsorption of  $H_2$ . For Pt based catalysts, these requirements are obviously optimized with Ru which, in contrast to Mo, Sn, Ni, Co, and Fe, at elevated temperatures shows some activity for the hydrogen oxidation process [99].

#### **4.2.4 Conclusions:**

This restricted review of a broad and expanding research field of electrocatalysis on metal surfaces represents an attempt to provide inside into the interrelationships between the kinetics of fuel cell reactions and the structure/composition of anode catalysts. Ex-situ UHV and in-situ SXS and FTIR studies in conjunction with the RDE method have been used to establish a link between the macroscopic kinetic rates and microscopic structure/site occupancy of intermediates and spectator adsorbates. Although an effort has been made to chose realistic illustrative examples for which there

are comparable experimental and theoretical work, some of conclusion presented herein are speculative and hopefully will stimulate further research.

It was proposed that two forms of the adsorbed H and CO can be distinguished on Pt(hkl) in an electrochemical environment: (i)  $H_{\text{opd}}$  and  $\text{CO}_{\text{ad}}$  with low heat of adsorption are characterized as the “weakly” adsorbed states, and (ii)  $H_{\text{upd}}$  and  $\text{CO}_{\text{ad}}$  with a relatively high enthalpy of adsorption are characterized as the “strongly” adsorbed states. These concepts for  $H_{\text{ad}}$  and  $\text{CO}_{\text{ad}}$  energetics and the transition from the weakly state into the strongly state are the keys to understanding the relation between reactivity and interfacial structures of Pt(hkl) and Pt-bimetallic surfaces. Not surprisingly, modern research has clearly shown that electrocatalytic reactions are invariably structure sensitive, i.e. the rate depends of the atomic/molecular scale morphology of the surface. There is, however, an interesting new feature to this story that has emerged: not only does structure sensitivity arise because of the structure sensitivity of the adsorption energy of the reactive intermediates to site geometry, but also from the sensitivity to site geometry of adsorption of spectator species. For example, the significant deactivation of the HER/HOR kinetics in alkaline vs. acid electrolyte is suggested to arise mainly due to the presence of  $\text{OH}_{\text{ad}}$  even close to the reversible potential for the hydrogen electrode in alkaline electrolytes. The same argument was used to explain a surprisingly high activity of Pt(111) for the oxidation of CO in alkaline solution, e.g. the reaction proceeds between adsorbed CO and OH, the latter forming selectively *in* the  $H_{\text{upd}}$  region at defect sites. In acid solution these sites are blocked by specific adsorption of anions and consequently CO oxidation potential is shifted towards much more positive potentials. These examples are used to demonstrate that the optimization of an electrocatalyst for specific inorganic reaction must accommodate many contributing factors, some understood, some not, and it is a complex task. It is even more complicated to understand how a reaction proceeds when pure gasses are mixed, as in the case for the oxidation of  $\text{H}_2/\text{CO}$  mixtures on Pt(111) and Pt-bimetallic surfaces. The  $\text{Pt}_3\text{-Sn(hkl)}$  system was used to demonstrate that even though a great deal has already been learned and trends are beginning to emerge with respect to relationships between surface structure/composition of catalysts and the kinetics of  $\text{H}_2/\text{CO}$  mixtures, there are a number of areas where more work is required before the detail mechanisms can be considered reasonably well understood. These



relationships are, however, of practical significance in the search for more CO tolerant catalysts.

### **Acknowledgments**

The author is deeply indebted to H. Gasteiger, C. Lucas, B. Grgur, T. Schmidt, V. Stamenkovic, V. Climent, A. Rodes, M. Arenz, and P. Ross for the years of pleasant and productive collaboration leading to this review. The author is pleased to acknowledge long-term support for his research from the Director, Office of Science, Office of Basic Energy Sciences, Division of Materials Sciences, U.S. Department of Energy, under contract DE-AC03-76SF00098.

## Reference List

1. W.R.Grove, *Philos. Mag.*, 14 (1839) 127.
2. K.J.Vetter, *Electrochemical Kinetics*, Academic Press, New York 1967.
3. B.E.Conway and J.O.M.Bockris, *J. Chem. Phys.*, 26 (1957) 532.
4. R.Parsons, *Trans. Farady Soc.*, 54 (1958) 1053.
5. H.Gerischer, *Bull. Soc. Chim. Belg.*, 67 (1958) 506.
6. S.Trasatti, *J. Electroanal. Chem.*, 39 (1972) 163.
7. S.Trasatti, *Surf. Sci.*, 335 (1995) 1.
8. E.Protopopoff and P.Marcus, *J. Chim. Phys.*, 88 (1991) 1423.
9. F.Will, *J. Electroanal. Chem.*, 112 (1965) 451.
10. A.T.Hubbard, R.M.Ishikawa, J.Katekaru, *J. Electroanal. Chem.*, 86 (1978) 271.
11. A.S.Homa, E.Yeager, B.D.Cahan, *J. Electroanal. Chem.*, 150 (1983) 181.
12. F.T.Wagner and P.N.Ross Jr., *J. Electroanal. Chem.*, 150 (1983) 141.
13. A.T.Hubbard, *Chem. Rev.*, 88 (1988) 633.
14. J.Clavilier, *J. Electroanal. Chem.*, 107 (1980) 211.
15. N.Markovic, M.Hanson, G.McDougall, E.Yeager, *J. Electroanal. Chem.*, 214 (1986) 555.

16. M.Wasberg, L.Palaikis, S.Wallen, M.Kamrath, A.Wieckowski, J. Electroanal. Chem., 256 (1988) 51.
17. Kibler L.A., M.Cuesta, M.Kleinert, D.M.Kolb, J. Electroanal. Chem., 484 (2000) 73.
18. I.M.Tidswell, N.M.Markovic, P.N.Ross, J. Electroanal. Chem., 376 (1994) 119.
19. C.Lucas, N.M.Markovic, P.N.Ross, Phys. Rev. Lett., 77 (1996) 4922.
20. K.Sashikata, N.Furuya, K.Itaya, J. Vac. Sci. Tech. A, B9 (1991) 457.
21. S.Tanaka, S.-L.Yua, K.Itaya, J. Electroanal. Chem., 396 (1995) 125.
22. K.Itaya, Progress in Surface Science, 58 (1998) 121.
23. B.M.Ocko, J.Wang, A.Davenport, H.Isaacs, Phys. Rev. Lett., 65 (1990) 1466.
24. I.M.Tidswell, N.M.Markovic, C.Lucas, P.N.Ross, Phys. Rev. B, 47 (1993) 16542.
25. D.M.Kolb, Progress in Surface Science, 51 (1996) 109.
26. K.Christmann, in *Electrocatalysis*, J.Lipkowski, P.N.Ross Jr. Editors, p. 1, Wiley-VCH, New York (1998).
27. N.M.Markovic, H.A.Gasteiger, P.N.Ross, J. Electrochem. Soc., 144 (1997) 1591.
28. N.M.Markovic, T.J.Schmidt, B.N.Grgur, H.A.Gasteiger, P.N.Ross Jr., R.J.Behm, J. Phys. Chem. B, 103 (1999) 8568.
29. G.Jerkiewicz, Progress in Surface Science, 57 (1998) 137.
30. M.W.Breiter, Ann. N. Y. Acad. Sci., 101 (1963) 709.

31. M.Breiter, *Electrochim. Acta*, 7 (1962) 25.
32. B.E.Conway, H.Angerstein-Kozlowska, H.P.Dhar, *Electrochim. Acta*, 19 (1974) 455.
33. B.E.Conway, H.Angerstein-Kozlowska, W.B.A.Sharp, *J. Chem. Soc. Faraday Trans.*, 74 (1978) 1373.
34. B.E.Conway and J.C.Currie, *J. Chem. Soc. Faraday Trans. 1*, 74 (1978) 1390.
35. O.Bernauer, J.Topler, D.Noreus, D.Hemplemann, *Int. J. Hydrogen Energy*, 14 (1989) 187.
36. N.M.Markovic and P.N.Ross, *Surf. Sci. Reports*, 286 (2002) 1.
37. P.Paredes Olivera and M.Patrito, in *Interfacial Electrochemistry, Theory, Experiment, and Applications*, A.Wieckowski, Editor, p. 63, Marcel Dekker, Inc., New York, Basel (1999).
38. S.Schuldiner, M.Rosen, D.R.Flinn, *J. Electrochem. Soc.*, 117 (1970) 1251.
39. K.Seto, A.Iannelli, B.Love, J.Lipkowski, *J. Electroanal. Chem.*, 226 (1987) 351.
40. H.Kita, S.Ye, Y.Gao, *J. Electroanal. Chem.*, 334 (1992) 351.
41. R.Gomez, A.Fernandez-Vega, J.M.Feliu, A.Aldaz, *J. Phys. Chem.*, 97 (1993) 4769.
42. N.M.Markovic, S.T.Sarraf, H.A.Gasteiger, P.N.Ross, *J. Chem. Soc. Faraday Trans.*, 92 (1996) 3719.
43. T.J.Schmidt, N.M.Markovic, P.N.Ross, *J. Electroanal. Chem.*, (2002), in press.

44. N.M.Markovic, B.N.Grgur, P.N.Ross Jr., J. Phys. Chem. B, 101 (1997) 5405.
45. V.Stamenkovic, N.M.Markovic, P.N.Ross Jr., J. Electroanal. Chem., 500 (2000) 44.
46. T.J.Schmidt, N.M.Markovic, P.N.Ross, J. Phys. Chem. B, 67 (2001) 1.
47. V.Stamenkovic and N.M.Markovic, Langmuir, 17 (2000) 2388.
48. J.H.Barber, S.Morin, B.E.Conway, J. Electroanal. Chem., 446 (1998) 125.
49. J.H.Barber and B.E.Conway, J. Electroanal. Chem., 461 (1999) 80.
50. B.E.Conway, in *Interfacial Electrochemistry - Theory, Experiment, and Applications* -, A.Wieckowski, Editor, p. 131, Marcel Dekker, Inc., New York (1999).
51. B.E.Conway and G.Jerkiewicz, Electrochim. Acta, 45 (2000) 4075.
52. M.Breiter, C.A.Knorr, R.Meggle, Z. Electrochem., 59 (1995) 153.
53. A.N.Frumkin and E.A.Aikasiyan, Dokl. Akad. Nauk SSSR, 100 (1995) 315.
54. N.V.Osetrova and V.S.Bagotzky, Élektrokhimiya, 9 (1973) 1527.
55. C.T.Campbell, J.A.Rodriguez, D.W.Goodman, Phys. Rev. B, 46 (1992) 7077.
56. M.Han, P.Mrozek, A.Wieckowski, Phys. Rev. B, 48 (1993) 8329.
57. C.S.Cameron, G.A.Hards and D.Thompsett, in A.R.Landgrebe, R.K.Sen, D.J.Wheeler (Eds.), Proceedings of the Workshop on Direct Methanol-Air Fuel Cells, **PV 92-14**, p. 10, The Electrochemical Society, Pennington, N.J., 1992.

58. A.Hamnett, *Phil. Trans. R. Soc. Lond. A*, 354 (1996) 1653.
59. B.Hammer and J.K.Norskov, in *Chemisorption and Reactivity on Supported Clusters and Thin Films*, R.M.Lambert, G.Pacchioni, Editors, p. 285, Kluwer Academic Publisher, (1997).
60. G.A.Attard and A.Bannister, *J. Electroanal. Chem.*, 300 (1991) 467.
61. J.Clavilier, M.J.Llorca, J.M.Feliu, A.Aldaz, *J. Electroanal. Chem.*, 310 (1991) 429.
62. M.Baldauf and D.M.Kolb, *Electrochim. Acta*, 38 (1993) 2145.
63. M.Baldauf and D.M.Kolb, *J. Phys. Chem.*, 100 (1996) 11375.
64. V.Climent, N.M.Markovic, P.N.Ross, *J. Phys. Chem. B*, 104 (2000) 3116.
65. N.M.Markovic, C.Lucas, V.Climent, V.Stamenkovic, P.N.Ross, *Surf. Sci.*, 465 (2000) 103.
66. H.Isaacs and M.Ito, *J. Electroanal. Chem.*, 358 (1993) 307.
67. H.Naohara, S.Ye, K.Uosaki, *J. Phys. Chem. B*, 102 (1998) 4366.
68. Kibler L.A., Kleinert.M., R.Randler, D.M.Kolb, *Surf. Sci.*, 443 (1999) 19.
69. W.Heiland and E.Taglauer, R.L.Park, M.Lagally, Editors, p. 299, Academic Press, Orlando, FL (1985).
70. M.Arenz, V.Stamenkovic, K.Wandelt, P.N.Ross, N.M.Markovic, *Surf. Sci.*, (2002), in press.

71. M.Ball, C.Lucas, V.Stamenkovic, P.N.Ross, N.M.Markovic, Surf. Sci., (2002), in press.
72. E.Budevski, G.Staikov, W.J.Lorenz, *Electrochemical Phase Formation and Growth - An Introduction to the Initial Stages of Metal Deposition*, VCH, Weinheim, New York, Basel, Cambridge, Tokyo 1996.
73. C.T.Campbell, Annu. Rev. Phys. Chem., 41 (1990) 775.
74. K.A.Friedrich, K.-P.Geyzers, U.Linke, U.Stimming, J.Stumper, J. Electroanal. Chem., 402 (1996) 123.
75. T.Kitamura, M.Takahashi, M.Ito, Surf. Sci., 358 (1989) 337.
76. S.C.Chang and M.J.Weaver, Surf. Sci., 238 (1990) 42.
77. A.Rodes, R.Gomez, J.M.Feliu, M.J.Weaver, Langmuir, 16 (2001) 811.
78. W.Akemann, K.A.Friedrich, U.Stimming, J. Phys. Chem., 113 (2000) 6864.
79. (a)K. Yoshioka, F. Kitamura, M. Takeda, M. Takahashi, M. Ito., Surf. Scien. 227 (1990) 90; (b) S.Zou, R.Gomez, M.J.Weaver, J. Electroanal. Chem., 474 (1999) 155.
80. A.Gil, A.Clotet, A.Ricart, F.Illas, B.Alvarez, A.Rodes, J.M.Feliu, J. Phys. Chem. B, 30 (2001) 7263.
81. M.Arenz, K.Wandelt, V.Stamenkovic, P.N.Ross, N.M.Markovic, Langmuir, (2002), in press.
82. M.Koper, R.A.van Santen, S.A.Wasileski, M.J.Weaver, J. Chem. Phys., 113 (2000) 4392.

83. P.Liu and J.K.Norskov, Fuel Cells, 1 (2001) 192.
84. T.E.Shubina and M.T.M.Koper, Electrochimica Acta, (2002), in press.
85. N.M.Markovic, B.N.Grgur, C.A.Lucas, P.N.Ross, J. Phys. Chem. B, 103 (1999) 487.
86. I.Oda, J.Inukai, M.Ito, Chem. Phys. Lett., 203 (1993) 99.
87. W.-F.Lin, M.S.Zei, G.Ertl, Chem. Phys. Lett., 312 (1999) 1.
88. I.Villegas and M.J.Weaver, J. Chem. Phys., 101 (1994) 1648.
89. I.Villegas, X.Gao, M.J.Weaver, Electrochim. Acta, 40 (1995) 1267.
90. C.A.Lucas, N.M.Markovic, P.N.Ross, Surf. Sci., 425 (1999) L381.
91. N.M.Markovic and P.N.Ross Jr., Cat. Tech., 4 (2000) 110.
92. A.Wieckowski and J.Sobkowski, J. Electroanal. Chem., 63 (1975) 365.
93. N.M.Markovic, C.A.Lucas, A.Rodes, V.Stamenkovic, P.N.Ross, Surf. Sci. Lett., 499 (2002) L149.
94. N.M.Markovic and P.N.Ross, Electrochim. Acta, 45 (2000) 4101.
95. N.M.Markovic, B.N.Grgur, C.A.Lucas, P.N.Ross Jr., Langmuir, 16 (2000) 1998.
96. M.Watanabe, M.Horiuchi, S.Motoo, J. Electroanal. Chem., 250 (1988) 117.
97. H.A.Gasteiger, N.Markovic, P.N.Ross, E.J.Cairns, J. Phys. Chem., 98 (1994) 617.
98. H.A.Gasteiger, N.Markovic, P.N.Ross, J. Phys. Chem., 99 (1995) 8290.
99. H.A.Gasteiger, N.Markovic, P.N.Ross, J. Phys. Chem., 99 (1995) 16757.



100. B.N.Grgur, G.Zhuang, N.M.Markovic, P.N.Ross Jr., J. Phys. Chem. B, 101 (1997) 3910.
101. B.N.Grgur, N.M.Markovic, P.N.Ross Jr., J. Phys. Chem. B, 102 (1998) 2494.
102. B.N.Grgur, N.M.Markovic, P.N.Ross Jr., J. Electrochem. Soc., 146 (1999) 1613.
103. S.Mukerjee, S.J.Lee, E.A.Ticianelli, J.McBreen, B.N.Grgur, N.M.Markovic, P.N.Ross, J.R.Giallombardo, E.S.De Castro, Electrochem. Sol. Let., 2 (1999) 12.
104. H.A.Gasteiger, N.M.Markovic, P.N.Ross, J. Phys. Chem., 99 (1995) 8945.
105. H.A.Gasteiger, N.M.Markovic, P.N.Ross Jr., Catal. Let., 36 (1996) 1.
106. D.P.Wilkinson and D.Thompsett, in O.Savadogo and P.R.Roberge (Eds.), Proceedings of the Second International Symposium on New Materials For Fuel Cell and Modern Battery Systems, p. 266, École Polytechnique de Montréal, Montréal, 1997.
107. M.Watanabe, Y.Zhu, H.Igarashi, H.Uchida, Electrochemistry, 68 (2000) 244.
108. H.Igarashi, T.Fujino, J.Zhu, H.Uchida, M.Watanabe, Phys. Chem. Chem. Phys., 3 (2001) 306.
109. J.M.Sinfelt, *Bimetallic Catalysts: Discoveries, Concepts and Applications*, Wiley, New-York 1983.
110. M.Watanabe and S.Motoo, J. Electroanal. Chem., 60 (1975) 275.
111. M.T.M.Koper, T.E.Shubina, R.A.van Santen, J. Phys. Chem. B, 106 (2002) 686.
112. B.Hammer and J.K.Norskov, Adv. Catal., 45 (2000) 71.

113. A.B.Anderson, E.Grantscharova, P.Shiller, J. Electrochem. Soc., 142 (1995) 1880.
114. J.Xu and J.T.Jates, J. Chim. Phys., 99 (1993) 725.
115. A.Szabo, M.A.Henderson, J.T.Yates, J. Chim. Phys., 96 (1996) 6191.
116. W.-F.Lin and S.G.Sun, Electrochim. Acta, 41 (1996) 803.
117. V.Stamenkovic, M.Arenz, P.N.Ross, N.M.Markovic, J. Phys. Chem. B, (2002), in press.
118. T.Engel and G.Ertl, Advances in Catalysis, 28 (1979) 1.
119. J.M.White and S.Akhter, in *Crit.Rev.Solid State Mater.Sci*, p. 131, CRC, (1988).
120. P.W.Faguy, N.Markovic, R.R.Adzic, C.A.Fierro, E.B.Yeager, J. Electroanal. Chem., 289 (1990) 245.
121. Y.Sawatari, J.Inukai, M.Ito, J. Electron Spec., 64/65 (1993) 515.
122. R.J.Nichols, in *Frontiers of Electrochemistry*; J.Lipkowski, P.N.Ross , Editors, p. 99, Wiley-VCH,Inc, New York (1999).
123. F.C.Nart, T.Iwasita, M.Weber, Electrochim. Acta, 39 (1994) 961.
124. A.Kabbabi, F.Gloaguen, F.Andolfatto, R.Durand, J. Electroanal. Chem., 373 (1994) 251.

**Table 1:** Thermodynamic state functions for  $H_{\text{upd}}$  on Pt(111) in 0.1 M KOH;  $r = 40$  kJ/mol. Note: thermodynamic state functions for  $H_{\text{upd}}$  in 0.1 M HClO<sub>4</sub>, and 0.05 M H<sub>2</sub>SO<sub>4</sub> are almost identical with one shown in Table 1 [].

Table 1

T [124]	$\Delta G^{\ominus=0}_{\text{Hupd}}$ [kJ/mol]	$f=r/(RT)$	$\Delta H_{\text{Hupd}}$ [kJ/mol]	$\Delta S_{\text{Hupd}}$ [J/mol*K]	$E_{\text{Pt-H}}$ [kJ/mol]
276	-24	16	-41	≈-63	≈240
303	-22	15			
333	-20	13			

**Table2:** Kinetic parameters for the HER/HOR on Pt(hkl) in 0.1 M KOH and, for comparison in 0.05 M H<sub>2</sub>SO<sub>4</sub>.(\*) At higher temperatures it was difficult to use any reliable fittings to extrapolate the  $i_0$  value. It was proposed that  $\Delta H^{0\#}$  for Pt(100) is between the one of Pt(111) and Pt(110).

	$i_0$ [mAcm <sup>-2</sup> ]				$\Delta H^{0\#}$ [kJmol <sup>-1</sup> ]	$i_0$ [mAcm <sup>-2</sup> ]		$\Delta H^{0\#}$ [kJmol <sup>-1</sup> ]
	0.1 M KOH					0.05 M H <sub>2</sub> SO <sub>4</sub>		
	275K	293 K	313 K	333 K		274K	333K	
<b>Pt(111)</b>	0.01	0.035	0.1	0.3	46	0.21	0.83	18
<b>Pt(110)</b>	0.125	0.3	0.56	0.675	23	0.65	1.35	9.5
<b>Pt(100)</b>	0.05	(*)	(*)	(*)	(*)	0.36	0.76	12

## FIGURE CAPTIONS:

**Figure 1.** Cyclic voltammograms of Pt(hkl) disk electrodes in 0.1 M KOH at 1600 rpm, 298 K, and sweep rate of 50 mVs<sup>-1</sup>. Charge evaluation deduced from CVs are represented by circles and squares.

**Figure 2.** Change of thermodynamic functions for H<sub>upd</sub> on Pt(111) in 0.1 M HClO<sub>4</sub> with surface coverage of H<sub>upd</sub> **(a)** apparent free energy of adsorption **(b)** apparent enthalpy of adsorption **(c)** apparent entropy of adsorption.

**Figure 3. (a)** Polarization curves for the HER and the HOR on Pt(111) in 0.05 M H<sub>2</sub>SO<sub>4</sub> at 900 rpm, 274 K, and 20 mV/sec. **(b)** Polarization curves for the HER and the HOR on Pt(111) in 0.05 M H<sub>2</sub>SO<sub>4</sub> 900 rpm, 333 K, and 20 mV/sec. **(c)** Arrhenius plots of the exchange current densities (*i*<sub>o</sub>) for the HER/HOR on Pt(hkl) in acid solution. **Inserts:** Polarization curves for the HER and the HOR in the micropolarization region at (a) 274 K and (b) 333 K.

**Figure 4. (a)** Polarization curves for the HER and the HOR on Pt(111) in 0.1 KOH at 2500 rpm, 274 K, and 20 mV/sec. **(b)** Polarization curves for the HER and the HOR on Pt(111) in 0.1 KOH, 2500 rpm, 333 K, and 20 mV/sec. **(c)** Arrhenius plots of the exchange current densities (*i*<sub>o</sub>) for the HER/HOR on Pt(hkl) in acid solution. **Inserts:** Ideal models of Pt(111), Pt(100) and Pt(110) structures. Small dots represents possible active sites for H<sub>upd</sub> and H<sub>opd</sub>.

**Figure 5. (a)** Cyclic voltammometry for Pt(111)-xPd (0 < x < 1 ML) in 0.05 M H<sub>2</sub>SO<sub>4</sub> at 298 K, and 50 mVs<sup>-1</sup> with various amounts of Pd deposited in UHV; **(b)-(e)** corresponding LIES spectra after Pd deposition; He<sup>+</sup> energy=1 keV; in (e) the LIES spectrum of Pt is included as a reference (dashed line).

**Figure 6.** Series of infrared spectra of  $\text{CO}_{\text{ad}}$  on (a) Pt(111), (b) Pt(111)-1ML Pd and (c) Pt(111)-43% Pd obtained by stepping the applied potential in a positive direction in CO saturated 0.1 KOH solution, each spectrum is accumulated from 50 interferometer scans at the potential indicated, the background potential was taken at 0.9 V vs. RHE.

**Figure 7.** Polarization curves for the HER and the HOR on Pt(111)-xPd in 0.05 M  $\text{H}_2\text{SO}_4$  at 900 rpm, 298 K, and 20 mV/sec. **Insert:** Arrhenius plots of the exchange current densities ( $i_0$ ) for the HER/HOR on Pt(hkl) in acid solution.

**Figure 8.** Polarization curves for the HER and the HOR on Pt(111)-xPd in 0.1 M KOH at 2500, 298 K, and 20 mV/sec. **Insert:** Cyclic voltammograms of Pt(111) (dashed) and Pt(111)-1MLPd (solid) in 0.1 M KOH at 298 K and 50  $\text{mVs}^{-1}$ .

**Figure 9.**  $I_k$  vs.  $\Theta_{\text{Pd}}$  relationship for the HOR in 0.05 M  $\text{H}_2\text{SO}_4$  at  $\eta = 0.25$  mV. Ideal models for pseudomorphic Pd (gray circles) layers on Pt(111) (dark circles).

**Figure 10.** (a) Potential-dependent stability of the  $\text{p}(2 \times 2)\text{-}3\text{CO}_{\text{ad}}$  structure on Pt(111) in 0.1 M  $\text{HClO}_4$  in CO-saturated solution, and  $\text{CO}_2$  production as a function of electrode potential (data extracted from FTIR measurements) during the oxidation of  $\text{CO}_{\text{ad}}$ . (b) Integrated intensities for  $\text{CO}_{\text{ad}}$ -atop,  $\text{CO}_{\text{ad}}$ -multi and  $\text{CO}_{\text{ad}}$ -bridge on Pt(111) as a function of electrode potential in CO-saturated 0.1 M  $\text{HClO}_4$  solution. (c) FTIR spectra obtained during progressive oxidation of  $\text{CO}_{\text{ad}}$  on Pt(111) in 0.1 M  $\text{HClO}_4$  from the initial potential, *ca.*  $E=0.05$  V. Each spectrum, displayed as relative reflectance ( $\Delta R/R$ ), was acquired from 100 interferometer scans at the range potential indicated, rationed to the corresponding spectrum obtained at the final potential, *ca.*  $E=0.9$  V.

**Figure 11.** (a) Potential-dependent stability of the p(2x2)-3CO<sub>ad</sub> structure on Pt(111) in 0.1 M KOH in CO-saturated solution, and CO<sub>2</sub> production as a function of electrode potential (data extracted from FTIR measurements) during the oxidation of CO<sub>ad</sub>. (b) Integrated intensities for CO<sub>ad</sub>-atop, CO<sub>ad</sub>-multi and CO<sub>ad</sub>-bridge on Pt(111) as a function of electrode potential in CO-saturated 0.1 M HClO<sub>4</sub> solution. (c) FTIR spectra obtained during progressive oxidation of CO<sub>ad</sub> on Pt(111) in 0.1 M HClO<sub>4</sub> from the initial potential, *ca.* E=0.05 V. Each spectrum, displayed as relative reflectance ( $\Delta R/R$ ), was acquired from 100 interferometer scans at the range potential indicated, rationed to the corresponding spectrum obtained at the final potential, *ca.* E=0.9 V.

**Figure 12.** (a) Potential-dependent stability of the p(2x2)-3CO<sub>ad</sub> structure on Pt(111) in 0.1 M HClO<sub>4</sub> + 10<sup>-2</sup> M Br<sup>-</sup> in CO-saturated solution, and CO<sub>2</sub> production as a function of electrode potential (data extracted from FTIR measurements) during the oxidation of CO<sub>ad</sub>. (b) Integrated intensities for CO<sub>ad</sub>-atop, CO<sub>ad</sub>-multi and CO<sub>ad</sub>-bridge on Pt(111) as a function of electrode potential in CO-saturated 0.1 M HClO<sub>4</sub> solution. (c) FTIR spectra obtained during progressive oxidation of CO<sub>ad</sub> on Pt(111) in 0.1 M HClO<sub>4</sub> from the initial potential, *ca.* E=0.05 V. Each spectrum, displayed as relative reflectance ( $\Delta R/R$ ), was acquired from 100 interferometer scans at the range potential indicated, rationed to the corresponding spectrum obtained at the final potential, *ca.* E=0.9 V.

**Figure 13.** Rocking scans through the ( $\frac{1}{2}$ ,  $\frac{1}{2}$ , 0.2) reciprocal lattice position, where scattering from the p(2x2)-3CO structure is observed, for (a) 0.1M HClO<sub>4</sub> + 10<sup>-2</sup> M Br<sup>-</sup>, (b) 0.1 M HClO<sub>4</sub> and (c) 0.1 M KOH. The solid lines are fits of a Lorentzian lineshape to the data which gives a coherent domain size for the p(2x2) structure of 350 Å, 130 Å and 30 Å in (a), (b) and (c) respectively. Also shown is a schematic picture of the p(2x2)-3CO unit cell.

**Figure 14.** Potentiodynamic CO<sub>b</sub> oxidation current densities on Pt(111) in 0.1 M HClO<sub>4</sub> + 10<sup>-2</sup> M Br<sup>-</sup>; 0.1 M HClO<sub>4</sub>; and 0.1 M KOH. Sweep rate 20 mV/s. Rotation rate 900 rpm.

**Figure 15.** CO stripping curve (solide) on Pt(111) in argon purged solution; CO was adsorbed at 0.05 V and the first sweep up to 0.5 V was recorded. Polarization curve for the HOR (dashed) on Pt(111) covered with 0.75 ML of CO<sub>ad</sub>.

**Figure 16.** Correlation between the rate of the HOR and the stripping charge for the oxidative removal of CO<sub>ad</sub> on Pt(100) and Pt(111) surfaces in 0.5 M H<sub>2</sub>SO<sub>4</sub>.

**Figure 17.** (a) Potentiodynamic CO oxidation current densities on Pt(111) in 0.5 M H<sub>2</sub>SO<sub>4</sub> saturated with CO. **Insert:** Magnification of the “pre-ignition” region. (b) Potentiodynamic CO oxidation current for the 2 %CO/Ar mixture on Pt(111). (c) Potentiodynamic HOR current density on Pt(111) in 0.5 M M H<sub>2</sub>SO<sub>4</sub> saturated with 2%CO/H<sub>2</sub> mixtures. Sweep rate was 5 mVs<sup>-1</sup>.

**Figure 18.** Series of infrared spectra during (a) CO<sub>2</sub> production and (b) progressive oxidation of CO on Pt<sub>3</sub>Sn(111) in 0.5 M H<sub>2</sub>SO<sub>4</sub> saturated with CO; each spectrum is accumulated from 50 interferometer scans at the potential indicated. (c) Integrated intensities for CO<sub>2</sub> production and CO<sub>ad</sub> as a function of electrode potential in CO-saturated 0.5 M H<sub>2</sub>SO<sub>4</sub> solution.

**Figure 19.** (a) Potentiodynamic CO oxidation rate, expressed as the turn over frequency(TOF), defined as the number of complete reaction events per active sites per second, on Pt<sub>3</sub>Sn(111) in 0.5 M H<sub>2</sub>SO<sub>4</sub> saturated with CO. (b) Cyclic voltammogram for Pt<sub>3</sub>Sn(111) in 0.5 M H<sub>2</sub>SO<sub>4</sub>. Potential dependence of corrected bisulfate integrated band intensities taken from spectra shown in (c). **Insert:** Ideal model of L<sub>1</sub>2 structure of Pt<sub>3</sub>Sn(111).

**Figure 20.** Positive-going potentiodynamic (1 mV/s) oxidation current densities for pure CO, 2% CO/H<sub>2</sub>, and 0.1% CO/H<sub>2</sub> (2500 rpm) at 62 °C: **(a)** UHV annealed (111) surface with  $x_{\text{Sn}} \approx 0.25$ ; and **(b)** (110) surface with  $x_{\text{Sn}} \approx 0.21$ . The dotted line indicates the potential at which a current density of 0.2 mA/cm<sup>2</sup> is reached (this potential under identical conditions of pure Pt corresponds to 0.8 V, 0.68 V and 0.5 V for pure CO, 2% CO/H<sub>2</sub>, and 0.1% CO/H<sub>2</sub>, respectively). **Insert:** logarithmic reaction order plots of current density vs. CO partial pressure at the identical electrode potentials.